Manuscript submitted to the Journal of Geophysical Research: Planets

Ephemeral Ice Clouds in the Upper Mesosphere of Venus

Benjamin. J. Murray[1], Thomas. P. Mangan[2], Anni Määttänen[3] and John. M. C. Plane[2]

[1] School of Earth and Environment, University of Leeds.

[2] School of Chemistry, University of Leeds.

[3] LATMOS/IPSL, Sorbonne Université, UVSQ Université Paris-Saclay, CNRS, Paris, France

Corresponding author: Benjamin Murray(b.j.murray@leeds.ac.uk)

Key Points:

- The upper mesosphere of Venus is frequently supersaturated with respect to both amorphous solid water and crystalline carbon dioxide ice
- There is a persistent layer of nano-scale amorphous solid water particles encircling Venus
- Short-lived carbon dioxide ice clouds sporadically form in the upper mesosphere

Abstract

The conditions in Venus' upper mesosphere at around 120 km have some similarities to the upper mesosphere of Earth and Mars where ice clouds form. Here we show, using published satellite products and numerical modelling, that the upper mesosphere of Venus is sufficiently cold that both H_2O and CO_2 can condense to form particles. In fact, we show that there is likely to be a competition between the direct nucleation of particles from the gas phase (homogeneous nucleation) and the nucleation on meteoric smoke particles (MSPs, heterogeneous nucleation). Amorphous solid water particles (ASW) are likely to nucleate first, resulting in clouds of nano-scaled particles at around 120 km globally. The temperatures can then become sufficiently low that CO_2 particles can nucleate either on MSPs or on ASW particles (>30% of the time poleward of 60°). Since the main component of the atmosphere is CO_2 these particles will grow and sediment on a timescale of 10-20 minutes. Mie calculations show that these Venusian mesospheric clouds (VMCs) should be observable by contemporary satellite instruments, although their short lifetime means that the probability of detection is small. We suggest that VMCs are important for the redistribution of meteoric smoke and may serve as a cold-trap, removing some water vapour from the very upper mesosphere of Venus, through the growth and sedimentation of cloud particles, and possibly reducing the loss of water to space.

Plain Language Summary

Venus is renowned for extreme heat at the surface and clouds composed of sulphuric acid encircling the planet; however, there are regions of Venus's atmosphere that are sufficiently cold to harbour ice clouds. In fact, the temperatures frequently fall to below 100 K at around 120 km altitude and under the right conditions we have shown that ice clouds composed of both water and carbon dioxide ices can form. We have used published data from satellites that orbit Venus to show that clouds composed of nanometer sized water ice particles may encircle the planet. The temperatures are so low in this part of Venus' atmosphere that the ice in these water ice particles likely lacks any crystalline structure, that is, it has an amorphous (liquid-like) structure. Furthermore, when the temperature falls below about 90 K, we have shown that carbon dioxide ice crystals can form on top of water ice crystals. Since the atmosphere of Venus is mainly made of carbon dioxide, these carbon dioxide crystals grow and fall rapidly. If we were lucky enough to see one of these short-lived sporadic clouds it would look a bit like a mares' tail cloud on Earth.

1 Introduction

The plausibility of ice clouds in Venus' atmosphere has been discussed as early as the 1950s (Menzel & Whipple, 1954). Through differing analyses of infrared absorption seen at 3 μm from high altitude balloon measurements in the 1960s, both Bottema et al. (1965) and Pollack and Sagan (1968) suggested water ice clouds could explain the observed absorbances, although a rebuttal by Rea and O'Leary (1968) suggested this was possible only if the ice particles were submicron in size. Turco et al. (1983) expanded on these predictions, suggesting that water ice clouds may be present in two layers: one between 80 and 100 km, resulting from freezing of sulphuric acid haze droplets; and another layer at Venus' mesopause (~120 km) consisting of water ice nanoparticles, possibly nucleated on meteoric dust particles.

Since the prediction of water ice clouds on Venus by Turco et al. (1983), our understanding of both the physics of ice cloud formation in planetary atmospheres and the structure and dynamics of the Venusian atmosphere have increased greatly. A range of satellite observations of lower altitude (≤ 100 km) sulphuric acid haze layers have since been made (Titov et al., 2018), and recent observations by instruments onboard the Venus Express satellite have highlighted extreme temperature minima in Venus' upper atmosphere (Mahieux et al., 2015).

Figure 1 illustrates an example of a typical cold temperature profile (green line) from the Solar Occultation in the InfraRed (SOIR) instrument onboard the Venus Express satellite (Orbit 669.1, taken at 81.6º latitude on the 19th February 2008 from Mahieux et al. (2015)). This profile includes the coldest region in Venus' atmosphere, with temperatures below 100 K from 118 – 125 km, and a temperature minimum of 64 K at 121 km. The blue line in Figure 1 shows the saturation temperature for H_2O with respect to amorphous solid water (ASW), assuming a water vapour concentration of 1 ppmv (the expected range in the Venusian upper atmosphere is 0.56 – 2.45 ppmv (Chamberlain et al., 2020)). This highlights that the atmosphere is sometimes significantly supersaturated with respect to ASW within the cold pocket. We show here the saturation (frost) point associated with ASW, rather than the stable crystalline hexagonal phase of ice I (ice I_h), because under these conditions in the upper atmosphere any ice formed should be amorphous (Mangan et al., 2021). The Turco et al. (1983) prediction of water ice clouds was based on an assumed water vapour concentration of 10 ppm at slightly lower altitudes than the example shown in Figure 1, but with a much higher temperature minimum of 110 K; this led to a many orders of magnitude smaller supersaturations than those shown in Figure 1. These atmospheric conditions for water ice evoke comparisons to Polar Mesospheric Clouds (PMCs) on Earth (Plane et al., 2015), and water ice clouds observed in the upper atmosphere of Mars (Stcherbinine et al., 2020). On Mars, upper mesospheric clouds are also thought to redistribute H_2O, although the process is not as effective as it might be if the growth of ice particles can quench the supersaturation (Fedorova et al., 2020); nevertheless ice cloud formation and sedimentation of ice crystals will limit the amount of water transported vertically.

Figure 1 also shows the saturation temperature for crystalline CO_2 ice (phase I), the phase that we expect cloud particles to be composed of under conditions in the upper mesosphere of Venus (Mangan et al., 2017b), even if nucleation occurs through a different phase. The primarily CO_2 atmosphere of Venus is sufficiently dense and the cold pocket sufficiently cold that the atmosphere is also supersaturated with respect to CO_2 ice around the temperature minimum at 121 km. These atmospheric conditions are again comparable to the Martian upper atmosphere, where gravity wave-induced cold pockets enable deposition of the primary atmospheric constituent, producing populations of micron-sized CO_2 ice particles (Listowski et al., 2014; Plane et al., 2018). At the time of Turco et al. (1983), CO_2 ice clouds were not considered as a possibility, given that the first confirmed observations of high-altitude CO_2 ice clouds on Mars were not made for another 20 years (Montmessin et al., 2006), and the temperature minima reported by Turco et al. (1983) were insufficient to produce supersaturated conditions with respect to CO_2 ice.

Despite being higher on Venus, if H_2O and/or CO_2 ice clouds formed around this temperature minimum they would exist in a region with striking similarities to the mesospheric clouds observed on Mars, quite possibly with similar nucleating particles available. Hence, building on the predictions of water ice clouds by (Turco et al., 1983), we propose that ice clouds,

comprising both H_2O and CO_2 ice, may form in Venus' upper atmosphere at around 120 km in altitude. In this paper, using the more extensive database of measurements for the Venus atmosphere that are now available, and applying our improved knowledge of high-altitude clouds on Earth and Mars, we examine the formation, growth and composition of H_2O and CO_2 ice clouds, and their detectability, in the upper atmosphere of Venus.

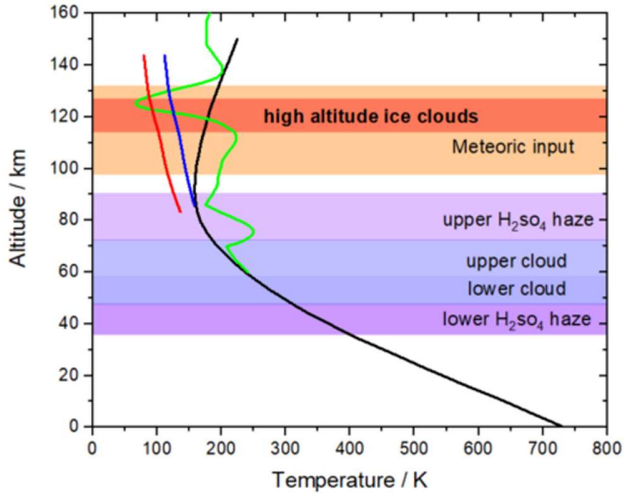

Figure 1. Atmosphere of Venus showing known and proposed cloud layers. General atmospheric profile (black) extracted from Palen et al. (2019). The temperature profile from orbit 669.1 (green) is taken from Mahieux et al. (2015). Saturation temperatures shown for H_2O with respect to amorphous solid water (blue) and CO_2 with respect to crystalline CO_2 (red). The water saturation ratios were calculated using the Nachbar et al. (2019) parameterisation for ASW in combination with the vapour pressure over hexagonal ice (Murphy & Koop, 2005). The frost point for crystalline CO_2 ice was calculated using saturation vapour pressure parameterisation from Azreg-Aïnou (2005). The altitude range over which meteoric ablation occurs is taken from Carrillo-Sánchez et al. (2020).

2. Nucleation of H2O and CO2 particles in Venus' mesosphere

To evaluate the feasibility of nucleation of H_2O and CO_2 ice particles in Venus' upper atmosphere we employ two theoretical approaches: Classical Nucleation Theory (CNT) and Kinetic Nucleation Theory (KNT). Atmospheres can exist in a metastable state where the partial pressure of some condensable component is greater than the equilibrium vapour pressure of a condensed phase (or phases) (Murray & Jensen, 2010). An atmosphere can persist in a supersaturated state because there is a free energy barrier to nucleation of a new phase related to the creation of a new interface. Nucleation can either occur spontaneously (homogeneous nucleation), or can occur at lower supersaturations on the surface of suitable particles. These ice-nucleating particles (INPs) stabilise the cluster of the condensed phase through favourable interactions with the surface. In cold clouds in Earth's mesosphere (Murray & Jensen, 2010), there is thought to be a competition between homogeneous and heterogeneous nucleation, and the balance between the mechanisms results in clouds with very different hydrometeor size

distributions. Sometimes heterogeneous nucleation occurring at lower supersaturations than those required for homogeneous nucleation leads to the depletion of the supersaturation as the ice particles grow, thus preventing homogeneous nucleation from occurring. But, if the cooling rate is sufficiently rapid then homogeneous as well as heterogeneous nucleation can occur (Murray & Jensen, 2010).

In the upper mesosphere of Venus there are at least two condensable materials, CO_2 and H_2O. The stable form of both of these materials is crystalline under the conditions on Venus, but it is unlikely that the critical cluster is made up of the stable phase. In many nucleating systems the initial phase to nucleate is a metastable phase that has a smaller surface energy penalty than the stable phase (Mullin, 2001). The metastable phase may subsequently relax to the stable phase. In the case of water homogeneously nucleating from water vapour, measurements clearly show that it is the liquid phase that nucleates at temperatures to below 200 K, even though the liquid phase rapidly converts to crystalline ice under those conditions (Wölk et al., 2013). At below around 120 K, deposition of water on a surface results in amorphous solid water (ASW); hence, the nucleating phase was probably amorphous but at these low temperatures the kinetics of transformation to the stable phase were too slow for it to occur on the experimental time scale (mins-hours) (Duft et al., 2019; Mangan et al., 2021). Similarly, for CO_2 recent experiments and molecular dynamics studies show that the initial phase to nucleate is a liquid-like form of CO_2 between 75 and 92 K (Dingilian et al., 2020; Halonen et al., 2021).

Heterogeneous nucleation requires the presence of particles on which nucleation might occur. The most likely candidate for particles that might serve as ice-nucleating particles (INPs) for ice clouds on Venus are nm-sized Meteoric Smoke Particles (MSPs). MSPs form from the recondensation of metallic compounds (oxides, hydroxides and carbonates) formed from the ablation of metals such as Fe, Mg and Na from cosmic dust particles entering an oxidizing planetary atmosphere such as Venus (Plane et al., 2015). Current predictions for Venus by Carrillo-Sánchez et al. (2020) show that ablation should occur between 100 and 125 km, peaking around 115 km (Figure 1). This altitude range happens to coincide with the cold pocket (Figure 1). In the following sections we use CNT and KNT to test the likelihood of both homogeneous and heterogeneous nucleation of both CO_2 and H_2O particles in the upper mesosphere of Venus. Note that there are also significant concentrations of HCl in Venus' upper mesosphere, approaching 1 ppm around 110 km and therefore ~ 1 – 10% of the H2O mixing ratio (Mahieux et al., 2015). HCl may therefore play a role as a condensable vapour, though this is likely to be as a minor enhancement of that of H2O.

2.1 Homogeneous nucleation of CO_2 and H_2O particles

Homogeneous nucleation directly from the vapour phase can occur under extreme conditions and it has been suggested that it may be important in the Earth's mesosphere (Lübken et al., 2009; Murray & Jensen, 2010). Given the conditions in the upper mesosphere of Venus are extremely cold, it is worth considering if H_2O or CO_2 particles might nucleate homogeneously. We have used a Classical Nucleation Theory (CNT) formulation described by (Määttänen et al., 2005). The equations and the choice of parameterisations of physical quantities are set out in Appendix A. Key physical quantities have been updated to be consistent with the latest experimental and theoretical studies. This includes the use of a parameterisation of the vapour pressure of ASW from Nachbar et al. (2019), who showed that ASW is not simply the low temperature extension

of supercooled liquid water and is in fact a distinct phase of water. We also derived a self-consistent interfacial energy for the liquid CO_2–vapour interface, based on measurements of homogeneous nucleation in a supersonic nozzle (Dingilian et al., 2020), and the ASW–vapour interfacial energy from studies of water uptake onto trapped nano-scale meteoric smoke analogues (Duft et al., 2019) (note that by self-consistent we mean that the interfacial energy is derived using the CNT and physical constant chosen in this paper, and then these CNT models are extrapolated to the conditions on Venus).

Nucleation rates (events per unit volume per unit time) for crystalline and amorphous/liquid-like phases of H_2O and CO_2 are shown in Figure 2a for an altitude of 121.6 km and a total pressure of 2.52 x 10^{-3} Pa (taken from the mean profiles derived from SOIR data in (Mahieux et al., 2015)). We assumed a water mixing ratio of 1 ppm and the CO_2 mixing ratio was taken as unity (in practice it is around 0.96). We also show, in **Figure 2**b, J_{hom} for one of the coldest temperature profiles in the SOIR dataset, 691.1 from the 12th March 2008 at 86.6° latitude from Mahieux et al. (2015), where the temperature minimum was 63 K at 121.6 km.

As expected, homogeneous nucleation of crystalline H_2O and CO_2 are very slow. In contrast, the homogeneous nucleation of ASW and liquid-like CO_2 might perhaps contribute to cloud particle populations. The nucleation rate for ASW is appreciable in this region, and is relatively insensitive to temperature with values of around 10^{-2} cm^{-3} s^{-1} at 63 K, which would produce ~1 cloud particle per cm^3 in 100 s. While there are uncertainties in the physical constants that go into the calculation of J_{hom}, J_{hom} in this 'plateau regime' has a relatively weak temperature dependence (**Figure 2**a) and is therefore insensitive to those uncertainties. Since the plateau value of J_{hom} is defined by the rate of formation of ASW clusters, which in turn is related to the H_2O monomer concentration, this limit should be well defined and it is unlikely that the true J_{hom} of ASW is many orders of magnitude larger (or smaller). The same cannot be said for J_{hom} for liquid CO_2 at around 120 km in the atmosphere of Venus. J_{hom} for liquid CO_2 has a very strong temperature dependence above ~60 K; hence, uncertainties in temperature and various physical quantities can have a substantial effect on the nucleation rate. For example, while J_{hom} is relatively small at 63 K, peaking at 10^{-5} cm^{-3} s^{-1} (Figure 2b), a shift of only 3 K to lower temperatures would increase J_{hom} to ~1 cm^{-3} s^{-1}. This would produce 100 particles per cubic centimetre in 100 s. Similarly, an interfacial energy only 15% smaller would also increase J_{hom} by more than five orders of magnitude. On this basis one should certainly not rule out homogeneous nucleation of liquid CO_2 particles, which would then rapidly convert to crystalline CO_2 ice.

To summarise, the role of homogeneous nucleation in clouds at around 120 km in the atmosphere of Venus, we can state that nucleation of crystalline particles cannot occur, whereas homogeneous nucleation of ASW and liquid CO_2 is feasible. The resulting CO_2 particles would likely rapidly crystallise, as was observed in experiments (Dingilian et al., 2020), whereas ASW would likely persist in an amorphous state (Mangan et al., 2021). The nucleation of ASW would proceed at a rate of up to 10^{-2} to 10^{-3} cm^{-3} s^{-1} in layers of ~4 km wide, depending on the shape of the temperature profile, whereas nucleation of CO_2 might produce very high number concentrations in very narrow layers at the locus of the temperature minimum, owing to the very strong temperature dependence of J_{hom}.

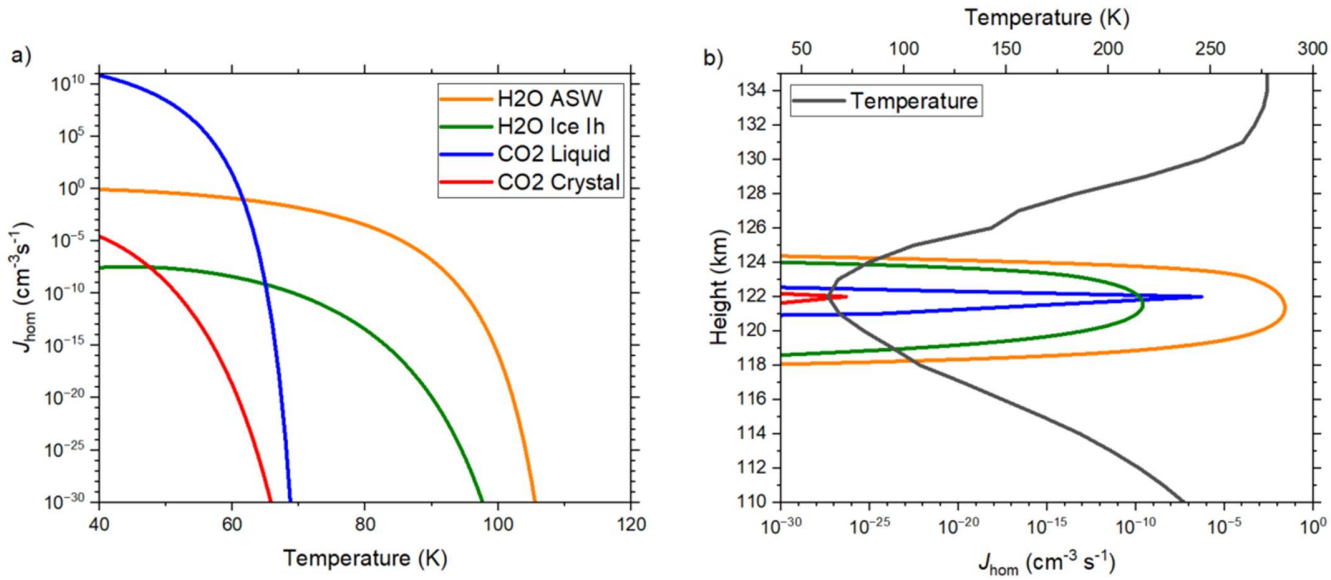

Figure 2. Homogeneous nucleation rates in the atmosphere of Venus. Panel a shows J_{hom} for CO_2 and H_2O particles in both an amorphous/liquid and crystalline form for an altitude of 121.6 km where the pressure was 2.51x10^{-3} Pa (from the average atmospheric profile for 80-90º latitude AM (AM refers to the morning terminator) in Mahieux et al. (2015)) and a mixing ratio of 1 ppm for H_2O and unity for CO_2. Panel b shows the corresponding J_{hom} values corresponding to the temperature and pressure profiles derived for SOIR profile 691.1, from the 12th March 2008 at 86.6° latitude from Mahieux et al. (2015).

2.2 Heterogeneous nucleation of CO_2 and H_2O particles

For mesospheric water ice clouds on Earth and Mars, the primary ice-nucleating particles for both planets are thought to be MSPs (Hervig et al., 2021; Plane et al., 2018). In Venus' atmosphere, metals such as Fe, Mg, Si and Na are modelled to ablate from dust particles of mostly cometary origin (within the altitude range shown in Figure 1 Carrillo-Sánchez et al. (2020). The metal atoms become oxidized and then polymerize into MSPs (Plane et al., 2018). To the best of our knowledge, no other particle sources are available above 100 km in Venus' atmosphere. Hence, MSPs are a likely candidate for nucleation of both CO_2 and H_2O particles.

The CNT formulation we adopt here has been used previously to evaluate nucleation of CO_2 and H_2O in Mars' upper atmosphere (Listowski et al., 2014; Listowski et al., 2013; Määttänen et al., 2005; Määttänen et al., 2007; Mangan et al., 2017b; Nachbar et al., 2016), but here we have updated the physical constants (see Appendix A). For CO_2 we use CNT to model the nucleation of crystalline ice on iron oxide or silica MSPs, and also on water ice. In addition, we use the KNT approach to study nucleation of CO_2 on metal carbonates, which are a more likely composition of MSPs in the CO_2 atmosphere of Venus (Plane et al., 2018). Since the KNT approach is somewhat different to CNT, we introduce it separately in section 2.4. Note that in

Venus' atmosphere these metallic carbonates and oxides may be partially converted to metal chlorides by the large concentrations of HCl present (Mahieux et al., 2015). However, electronic structure theory calculations of the kind described in Section 2.4 show that polar metal chlorides would be even more effective nuclei for CO_2 and H_2O, if they form. **Figure 3**a shows the probability of nucleation in one second as a function of temperature for the four potential nucleation pathways based on CNT. Three of these pathways involve MSPs (0.4 nm radius): nucleation of ice I_h is defined by the experiments of (Saunders et al., 2010) who quantified ice nucleation on MSP analogues in a cloud chamber at temperatures down to 180 K, reporting m = 0.985 at 190 K (θ = 10°); nucleation of ASW on MSPs is defined by the experiments of (Duft et al., 2019) who studied absorption and particle growth kinetics between 128 and 147 K, showing ASW was indeed the phase to nucleate under these conditions and surface adsorption of water resulting in an m of ~1; and nucleation of CO_2 on MSPs composed of iron oxides or silica was defined by (Nachbar et al., 2016) between 64 and 73 K, reporting $m = 0.78 \pm 0.02$. In addition we illustrate the nucleation of CO_2 on H_2O ice particles of 1 nm and 5 nm radius, where nucleation was defined experimentally by (Glandorf et al., 2002) between 130 and 140 K, finding m = 0.95. Details of each of these CNT formulations are given in Appendix A.

Inspection of the nucleation probabilities in **Figure 3**a shows that the nucleation of ASW on 0.4 nm MSPs is most favourable, with nucleation probability increasing from an infinitely small value to unity on decreasing the temperature by only a few degrees. This occurs at a saturation ratio with respect to ASW of ~250, and larger MSPs would be expected to nucleate at even lower supersaturations. A nucleation probability of unity means that 100% of 0.4 nm MSP particles would activate to create ASW particles, hence consuming all MSPs before CO_2 or ice I_h might nucleate on them. If the MSP particle concentrations were 100 cm^{-3}, then a cloud of 100 ASW particles would nucleate and grow. These particles would only grow to a few nanometers given the availability of H_2O in the rarefied upper atmosphere of Venus. If the atmosphere were to become sufficiently cold, the curves in **Figure 3**a suggest that CO_2 might then nucleate on these small ASW particles. CO_2 is much more abundant than H_2O, and these particles would then grow rapidly (this is explored in more detail in Section 3 below).

We examine heterogeneous nucleation corresponding to a specific SOIR profile (691.1) in **Figure 3**b. The probability of nucleation in one second is shown for the nucleation of ASW on MSP and for CO_2 on ice. We do not show the probability of nucleation of ice I_h or CO_2 on MSP because according to these calculations all the MSP would be activated to form ASW particles long before the saturation was great enough for these other pathways to become active. It can be seen in **Figure 3**b that a broad layer of nanoscale ASW particles will form between 118 km and 125 km. The ASW saturation point is around 120 K at 122 km, hence these ASW particles will persist until the temperature goes above this threshold or when they slowly sediment out of the layer. SOIR profile 691.1 is a particularly cold profile and under these conditions nucleation of CO_2 on ASW particles becomes favourable between 120 and 123 km. Nucleation of CO_2 on ice will occur at temperatures below 80 K for 1 nm particles and below 89 K for 5 nm particles (**Figure 3**a), but in an increasingly narrow layer when the temperature minimum is less deep.

In summary, heterogeneous nucleation of ASW on MSPs is an effective pathway of producing water ice cloud particles in the upper atmosphere of Venus according to the parameterisation defined by the experiments of Duft et al. (2019). However, due to the limited availability of water vapour, these ASW particles will remain less than around 5 nm in radius, but fill a layer ~5

km thick. The number of heterogeneously nucleating ASW particles will be limited by the concentration of MSPs, but homogeneous nucleation of ASW may provide additional particles (we explore this in section 2.3). If the temperature then decreases sufficiently, CO_2 will nucleate on these nanoscale ASW particles at a temperature dependent on their size. These CO_2 particles have the potential to grow rapidly and this will be explored in section 3.

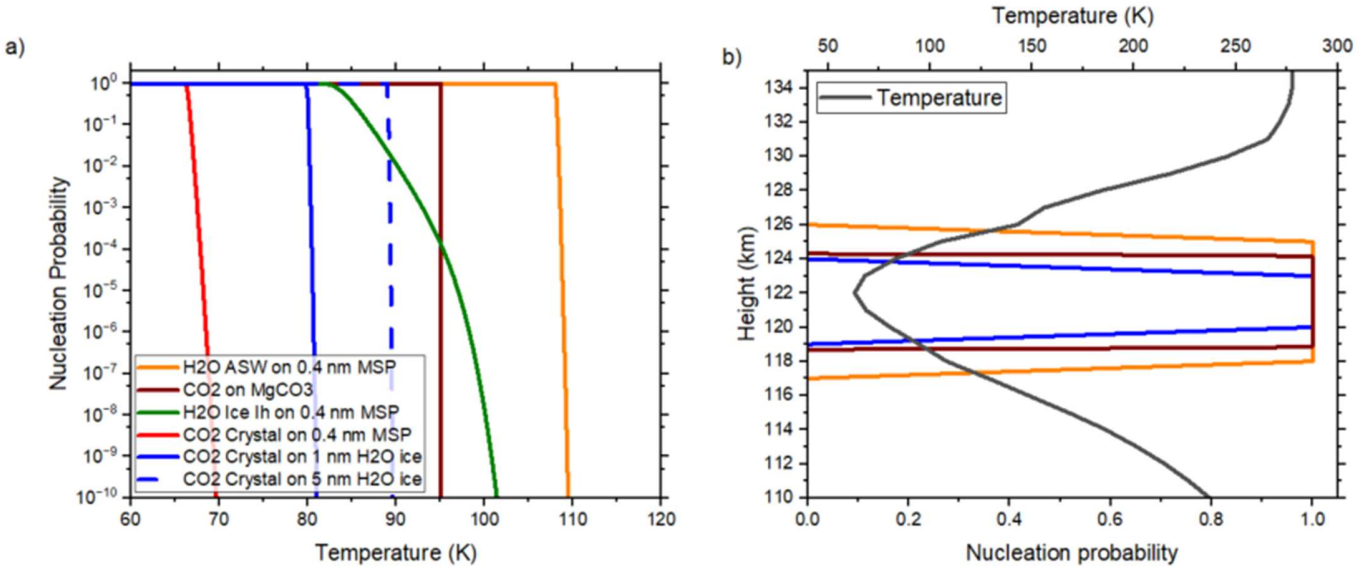

Figure 3. Probability of heterogeneous nucleation in the atmosphere of Venus. The nucleation probability is defined as the fraction of particles of defined size that nucleate ice in one second. a) The probability, from our CNT formulation, of H_2O or CO_2 nucleating on MSPs (0.4 nm radius) or H_2O ice particles (1 nm and 5 nm radius) as a function of temperature, as well as the onset of particle growth from the KNT model of CO_2 on $MgCO_3$ MSPs. These values correspond to an altitude of 121.6 km where the pressure was 2.51×10^{-3} Pa (from the average atmospheric profile for 80-90º latitude morning terminator in Mahieux et al. (2015)) and a mixing ratio of 1 ppm for H_2O and unity for CO_2. b) The nucleation probability corresponding to the temperature and pressure profiles derived for SOIR profile 691.1, from the 12th March 2008 at 86.6° latitude from Mahieux et al. (2015). We show the nucleation probabilities according to two potential mechanisms of CO_2 ice particle formation: first, is the direct nucleation of CO_2 on MSP according to KNT (section 2.4), and second, the nucleation of ASW on MSP followed by the nucleation of CO_2 on H_2O ice (section 2.1 and 2.2).

2.3 Competition between homogeneous and heterogeneous nucleation of ASW

We have shown that both homogenous and heterogeneous nucleation of ASW particles are feasible in the upper atmosphere of Venus. Here we examine which of these two mechanisms is likely to be more important in producing ice particles. In Figure 4 we show the number concentration of ASW particles resulting from both homogeneous and heterogeneous nucleation after 1 hr of constant conditions defined by SOIR profile 691.1. The number that nucleates heterogeneously is defined by the concentration of available MSP particles, which we have set at

100 cm^{-3} here. This number is insensitive to time, since for most of the cloud layer the probability of nucleation is unity for a 1 second interval. In contrast the number concentration of particles that nucleate homogeneously increases in proportion with time. For SOIR profile 691.1, homogeneous nucleation produces around 3 cm^{-3} ASW particles in one hour, whereas heterogeneous nucleation produces far more (depending on the assumed MSP concentration). If the cold pocket persisted for a day one would expect (3 cm^{-3} x 24) 72 cm^3 ASW particles over the course of the day. Sedimentation would then deplete the concentration, but there would be a persistent ASW production until the growth of ASW particles depleted the water partial pressure. In addition, it might be expected that cloud formation and sedimentation might deplete the MSP particle population, making homogeneous nucleation relatively more important. Given the uncertainties in the rate of homogenous nucleation and temperature measurements in Venus' atmosphere, as well as the MSP concentration, we cannot rule homogeneous nucleation out as making a significant contribution to the ASW particle population however, if MSP are present then the calculations indicate that heterogeneous nucleation will produce the majority of ASW particles in the upper atmosphere of Venus.

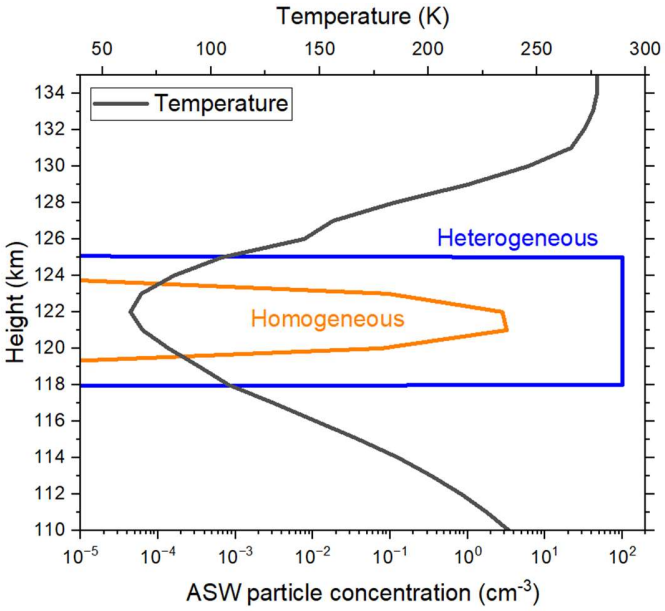

Figure 4. The competition between homogeneous and heterogeneous nucleation of ASW particles assuming conditions remain constant for 1 hour. The number concentration resulting from heterogeneous nucleation is defined by the product of probability of nucleation and the number concentration of MSP particles of 0.4 nm (which we assume is 100 cm^{-3}). The temperature and pressure profile correspond to SOIR profile 691.1.

2.4 CO_2 particle formation on carbonate MSPs from Kinetic Nucleation Theory

In the section above we established that a plausible mechanism for the formation of CO_2 ice particles is via the nucleation of ASW and the subsequent nucleation of CO_2 on those nanoscale ASW particles. Here we further explore the direct formation of CO_2 ice on MSP. In Figure 3a

we showed, based on the data of Nachbar et al. (2016), that nucleation on MSP composed of iron oxides and silica occurred 40 K lower than ASW on MSPs; hence is unlikely to be an important process. However, in a CO_2 rich atmosphere like that of Venus we expect meteoric smoke and MSPs to be composed of metal carbonates rather than oxides (Plane et al., 2018), and hence we need to consider the nucleation of CO_2 ice on metal carbonates. We were not able to find the pertinent physical data for the wetting properties of metal carbonate MSPs, so instead have used KNT. KNT is a bottom-up approach where the kinetics of adsorption and desorption of molecules to a cluster are treated explicitly (Bromley et al., 2016).

In these calculations the INP were assumed to be $MgCO_3$ and $FeCO_3$ which have already been discussed as likely MSP building blocks in the analogous atmosphere of Mars (Plane et al., 2018). The size of these seed particles was fixed at a radius of 0.35 nm, corresponding to a single $MgCO_3$ molecule with three CO_2 molecules bound to it (Plane et al., 2018). Because of the very large dipole moment of $MgCO_3$ (μ_D = 11.6 Debye), these CO_2 molecules are strongly enough bound for the $MgCO_3(CO_2)_3$ complex to be stable at temperatures below 150 K (Plane et al., 2018). Rate coefficients for the addition of subsequent CO_2 molecules up to $MgCO_3(CO_2)_{40}$ were then calculated using Rice Ramsperger Kassel Markus (RRKM) theory (Gilbert & Smith, 1990) with a solution of the Master Equation based on the inverse Laplace transform method (De Avillez Pereira et al., 1997). Electronic structure theory calculations (Frisch et al., 2016) were used to compute the vibrational frequencies of the small clusters up to $n = 4$. See Appendix B for details of these calculations and the derivation of the uptake coefficient, γ, for CO_2 attachment to an $MgCO_3(CO_2)_n$ cluster, and the rate of evaporation of the new cluster (i.e. $MgCO_3(CO_2)_{n+1} \rightarrow MgCO_3(CO_2)_n + CO_2$). Although γCO_2 is estimated to approach unity for cluster sizes larger than $n = 15$ at temperatures below 150 K (Figure B1a), we limit the value here to $\gamma CO_2 \leq 0.1$ to allow for the high pressure limiting attachment rate of CO_2 for $MgCO_3(CO_2)_n$ being lower than the hard sphere collision frequency (Smith, 1980). γCO_2 and the evaporation rate were computed at a pressure of 1.33 x 10^{-3}Pa (10^{-5} Torr), which is the typical pressure at ~150 km in Venus' atmosphere (Mahieux et al., 2015). γCO_2 at a lower altitude was then scaled by the relative atmospheric density, up to the limit of 0.1. The evaporation rate was then computed by detailed balance with the CO_2 attachment rate, with an equilibrium constant calculated by statistical mechanics with the partition functions for $MgCO_3(CO_2)_{n+1}$ and $MgCO_3(CO_2)_n$ using the vibrational frequencies and rotational constants described in the SI. For clusters larger than $n = 40$, γCO_2 was set to 0.1 at all temperatures below 180 K, and the equilibrium constant (and hence the evaporation rate) estimated from the Antoine relation for gas-phase CO_2 above the solid (Chicko, 2022; Giauque & Egan, 1937).

The conditions under which CO_2 particle growth becomes favourable are indicated in **Figure 3**. MSPs can provide a site where a CO_2 cluster is stabilised leading to growth of CO_2 particles at temperatures below about 95 K at 122 km. The initial cluster is non-crystalline, but on subsequent growth this material is likely to deposit as crystalline CO_2. However, if heterogeneous nucleation of ASW particles is as effective as indicated by our CNT formulation and the study of Duft et al. (2019), then the majority of MSP particles would already have activated to form nanoscale ASW particles. On the other hand, if the atmosphere were dehydrated by a previous cloud event, then new MSP particles might nucleate CO_2 in preference to ASW. Nevertheless, the most likely route to CO_2 particles is nucleation of CO_2 on ASW particles.

385 2.5 Planetary wide viability of H_2O and CO_2 ice particle formation

386 In order to assess the geographical distribution and occurrence frequency of cloud formation
387 conditions, we have plotted the SOIR profiles from Mahieux et al. (2015), broken down into
388 latitude bands and morning or evening terminator, in **Figure 5**. The SOIR temperature profiles
389 are then compared to the threshold temperatures at which ASW and crystalline CO_2 become
390 saturated (the phases that are expected to make up clouds) as well as the temperature at which
391 the nucleation rate of ASW on 1.0 nm ASW particles and CO_2 on 5 nm ASW particles is equal to
392 1 s^{-1} (equivalent to a nucleation probability in 1 s of 0.63).

393 While there is considerable variability of the temperature profiles, many of the profiles exhibit a
394 minimum around 120-130 km with a value below the temperature required for the nucleation and
395 persistence of both ASW and CO_2 ice particles (see **Figure 5** and **Figure 6**). On average across
396 all latitudes, 64% of the profiles indicate that the atmosphere is supersaturated with respect to
397 ASW in a layer ~5-10 km deep. Nucleation of ASW on MSPs is also possible in 51% of the
398 profiles on average. The sedimentation velocity of a 5 nm ASW particle at 120 km is 0.7 m s^{-1},
399 hence these particles would form a layer 5-10 km layer thick and have a lifetime with respect to
400 sedimentation on the order of hours. This indicates that clouds composed of nanoscale ASW
401 particles should be a regular feature of the atmosphere of Venus at around 120 km at all latitudes.
402 Nucleation of CO_2 on ASW particles is also remarkably frequent, occurring in 27 % of the
403 profiles on average. The frequency of CO_2 nucleation has a latitude dependence, with ~30-40%
404 of profiles between 60°-90° dipping below the threshold required for nucleation of CO_2 on 5 nm
405 ASW particles. Even at low latitudes (0-30°), ~8% of profiles were sufficiently cold for
406 nucleation of CO_2 on ASW. Hence, CO_2 cloud formation is also relatively frequent at all
407 latitudes. We now turn our attention to the properties and lifetime of these clouds and if they
408 should be observable with contemporary satellite instruments.

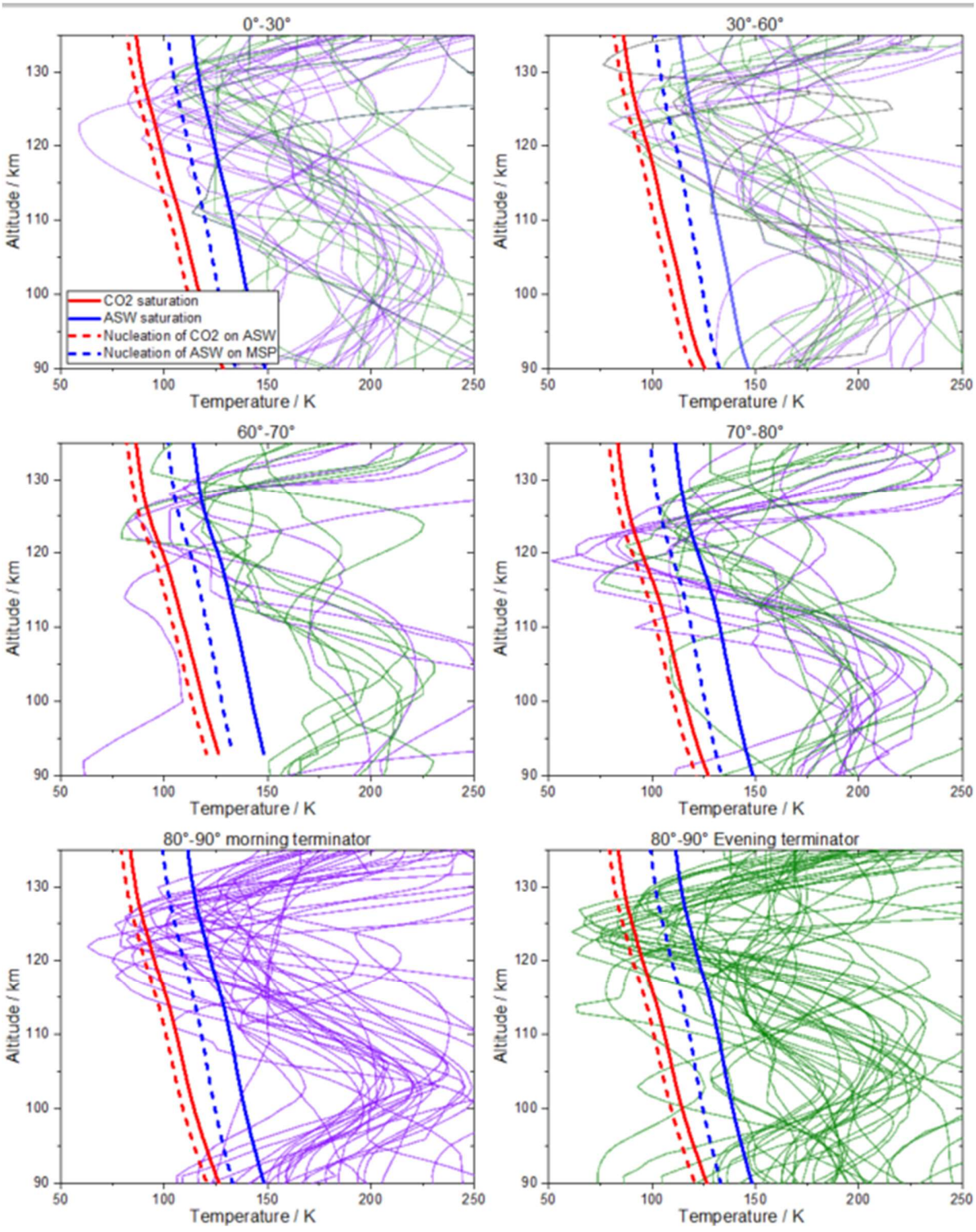

409

410 **Figure 5.** Latitude (0-90°) and time of day dependence (morning terminator in purple or evening
411 terminator in green) of saturation point temperature for crystalline CO_2 and ASW and of the
412 nucleation activation temperatures (where J_{het} = 1 s^{-1}, corresponding to a nucleation probability
413 of 0.63 in 1 s; we show values for nucleation of ASW on 1.0 nm MSP particles and CO_2 on 5 nm

414 ASW particles). Temperature profiles are taken from Mahieux et al. (2015) and the mean
415 morning terminator pressure profiles from the same paper are used to derive the saturation
416 temperatures and the nucleation activation temperatures.

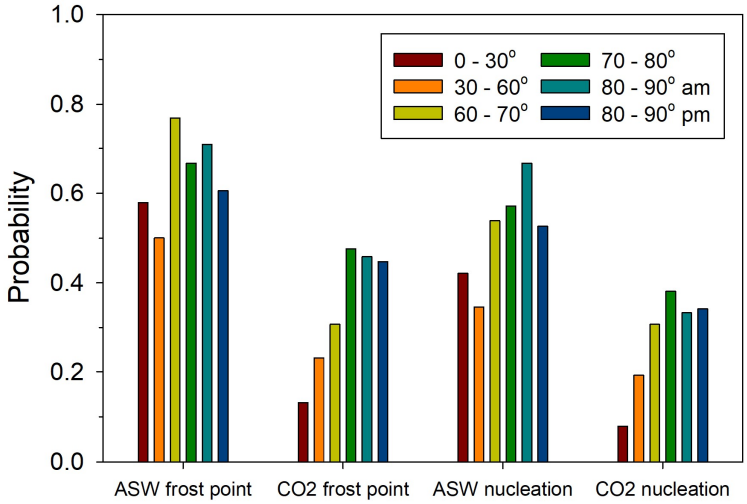

417

418 **Figure 6.** Probability of atmospheric temperature falling below the H_2O and CO_2 frost points,
419 and that required by CNT for particle nucleation above 100 km, using the observed temperature
420 profiles from the data set of Mahieux et al. (2015). The probability is defined as the fraction of
421 individual SOIR profiles where the temperature dropped below the respective frost point or
422 nucleation threshold (see Figure 5). These probabilities are cumulative, meaning that when the
423 SOIR temperature profile being below the CO_2 frost point, for example, the atmosphere is also
424 supersatured with respect to ASW.

425

426 **3 Modelling ice particle evolution in Venus' upper atmosphere**

427 In order to explore the evolution of the CO_2-ice clouds (the VMCs), a 1-dimensional
428 model was constructed which describes the nucleation, growth, sedimentation and sublimation of
429 the ice particles. The model is described in appendix C. The model is initiated with vertical
430 profiles of atmospheric density and temperature determined using the SOIR instrument (Mahieux
431 et al., 2015) that had a deep temperature minimum (< 90 K) so that CO_2 would have been highly
432 supersaturated. Figure 3 shows that under these conditions nucleation of CO_2 ice particles
433 occurs, either directly on MSPs or on ASW particles that had earlier nucleated on MSPs. Since
434 the concentration of ASW particles depends on the concentration of MSP particles both
435 pathways to formation of CO_2 ice particles would produce similar VMCs. Hence, our 1-D
436 microphysical model produces CO_2 ice crystals through the direct nucleation on MSP, but the
437 results would be similar for the case where CO_2 nucleates on ASW particles. Once CO_2 particles
438 are nucleated, the model follows the fate of the particles as they grow, sediment and finally
439 sublimate on entering a warmer region.

Figure 7 shows examples of model output, corresponding to two examples of cloud that can be produced from the observed SOIR temperature profiles. The first example peaks around 120 km with particles around 100-200 nm radius; and the second type persists for longer and peaks around 110 km, with particles that can exceed 2 μm in radius. The first cloud category is produced by deep, but relatively sharp temperature minima above 120 km (e.g. orbit 671.1). In contrast, the much larger particles in the second cloud category are produced by much broader temperature minima, in this case between ~112 and 122 km (e.g. orbit 1581.1). Figure 7b shows the time evolution of the particle size and height, for these two examples. The first cloud only lasts for ~350 s, and the second type lasts for around 1200 s (20 mins). The latter example is the most pronounced cloud that was generated in the model from the SOIR dataset (orbit 1581.1 at 87.3° on the 19th August 2010), but is still relatively short-lived because sedimentation is so rapid in this altitude range. Figure 8 also illustrates a composite of clouds predicted for multiple SOIR profiles at 70-80° and 80-90° bands (north and south), showing that these clouds all have similar features, with small CO_2 particles at higher altitudes that rapidly grow and sediment until they sublime 5-10 km below the cold point. Note that the depth of clouds at 80-90° is generally greater than clouds at 70-80°, as a result of the broader temperature minimum at higher latitudes.

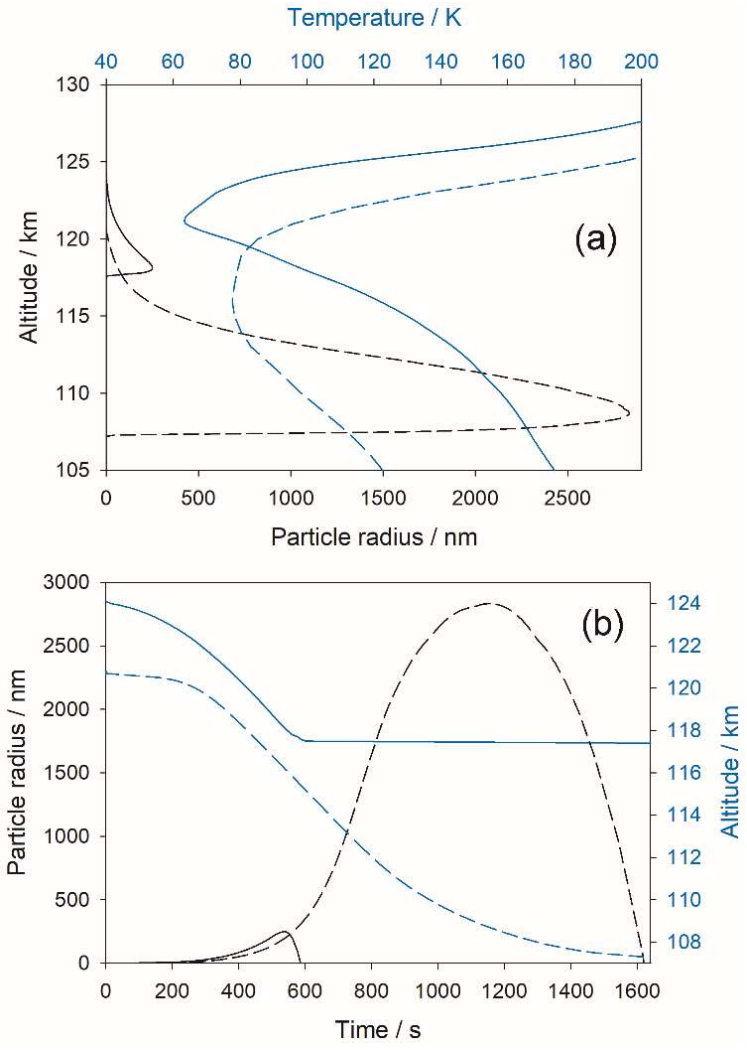

458

459

460 **Figure 7.** The microphysics of CO_2 ice clouds (a) Modelled CO_2 particle nucleation, growth,
461 sedimentation and sublimation for the temperature profile of orbit 671.1 at 82.9° (solid lines),
462 and orbit 1581.1 at 87.3° (dashed lines). (b) Time evolution of the radius and height of the CO_2
463 particles (γCO_2 = 0.1, MSP concentration = 100 cm^{-3}).

464

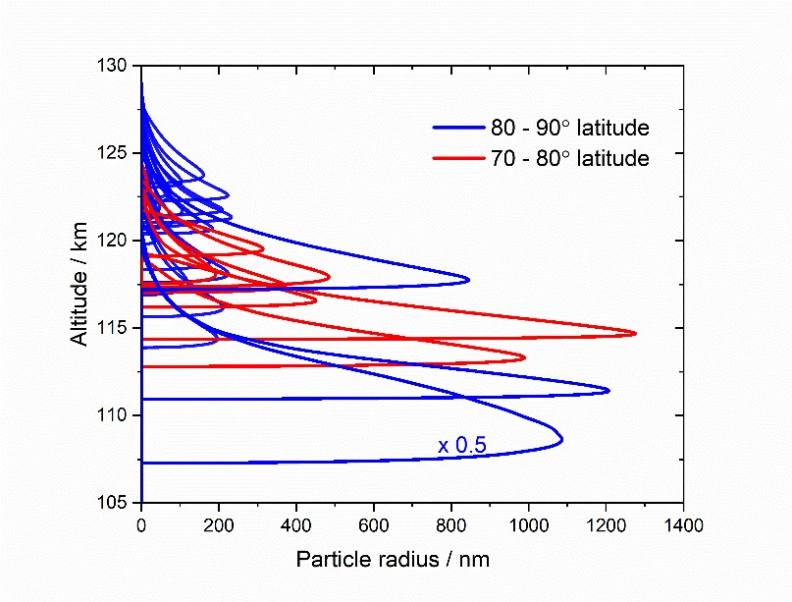

Figure 8. Modelled particle nucleation, growth and sedimentation of CO_2 particles initiated with multiple observed temperature profiles from the dataset of Mahieux et al. (2015) using $\gamma CO_2 =$ 0.1 at varying latitude ranges.

4 Detectability of CO_2 ice clouds

We have shown that conditions exist in the upper mesosphere of Venus where CO_2 clouds composed of ice particles in the 100s nm to micron sizes can form. We now address the question of whether these VMCs should be observable. The best chance of detection is likely through satellite observations of optical extinction. In this section we evaluate the possibility of detecting these high-altitude clouds in existing datasets by calculating the extinction by CO_2 ice particles using Mie theory. Venus Express had a suite of three instruments onboard that profile cloud and haze layers at lower altitudes on Venus. The first two are the UV and near-IR channels of the SPICAV instrument (Spectroscopy for the Investigation of the Characteristics of the Atmosphere of Venus) (although we do not include the near-IR channel in our current analysis). The UV channel has a wavelength range of 118-320 nm, and it performs stellar and solar occultations in addition to nadir and limb observations. The third instrument is SOIR (Solar Occultation in the InfraRed) which measures across the near- to mid-IR from 2.2-4.3 um (or 2200-4400 cm^{-1}) in solar occultation only. SPICAV has provided observations of the cloud and haze layers of Venus (Luginin et al., 2016; Wilquet et al., 2012; Wilquet et al., 2009), and SOIR observations were used also by Wilquet et al. (2009, 2012) and (Takagi et al., 2019). (Takagi et al., 2019) observed an increase in aerosol mixing ratio above 100 km, whereas the other studies reported results on clouds and hazes only at altitudes below 100 km. For the purposes of our Mie calculations we have selected the wavelength at 220 nm for SPICAV-UV and at 3320 nm for SOIR; both instruments have a similar detection limit around 1×10^{-5} km^{-1} (Wilquet et al., 2009).

We evaluate the detection probability of H_2O core (1 nm radius) CO_2 shell particles that might form in at an altitude of 120 km by determining the Mie extinction cross sections of individual

particles as a function of radius. We use refractive indices for CO_2 taken from Warren (1986), and those for water ice at 220 nm and 3320 nm from Kofman et al. (2019) and Warren and Brandt (2008), respectively. At 220 nm the water ice refractive indices were measured specifically for low density amorphous (LDA) ice at 70 K (Kofman et al., 2019).

In Figure 9 we show the extinction for CO_2 particles at varying radii and particle concentrations. Figure 7 shows that CO_2 particles often grow into the 100s nm range, hence extinction above the detection limit at both 220 nm and 3320 nm is possible with a sufficiently high number concentration. However, at 220 nm extinction exceeds the detection limit for much smaller particles and for lower number concentrations. For example, for CO_2 ice particle concentration of 100 cm^{-3}, detection at 220 nm using SPICAV-UV would occur when the particles were larger than ~25 nm, whereas for detection at 3320 nm with SOIR the particles would need to be above ~160 nm.

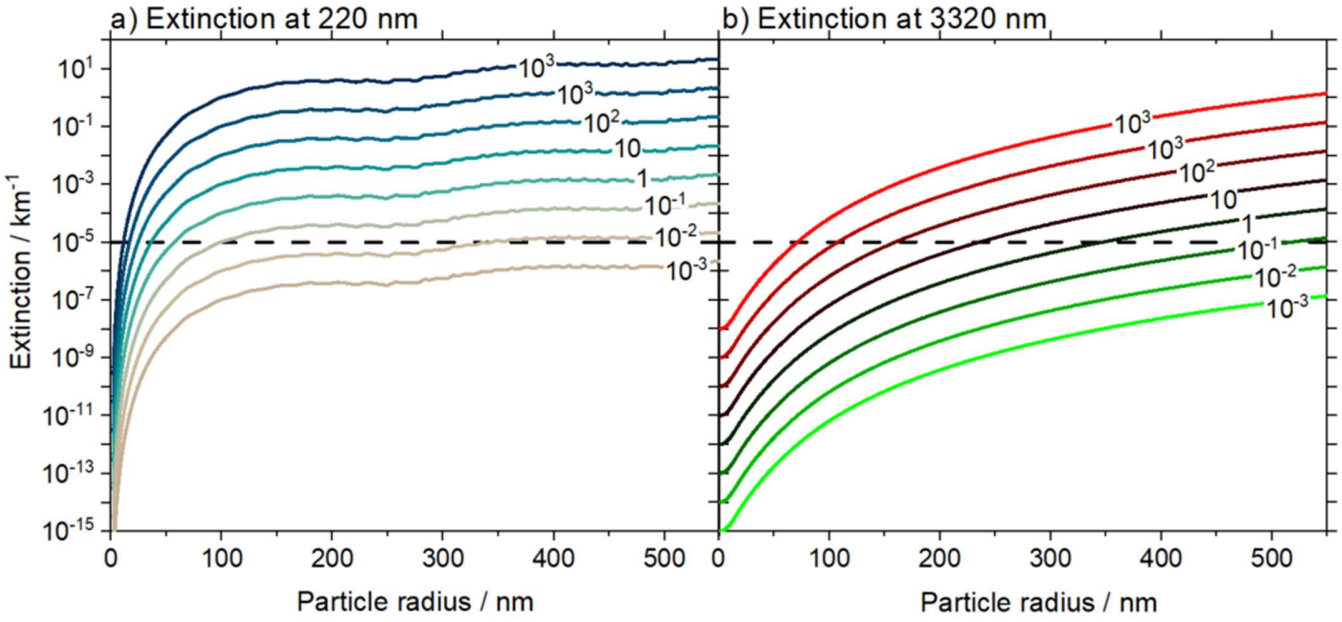

Figure 9. Predicted extinction coefficients in km^{-1} for VMCs with particle radius for different particle concentrations at 220 nm (a) and 3320 nm (b) for CO_2 particles with 1 nm radius H_2O cores. The dotted line shows the detection limits 1×10^{-5} km^{-1} for SPICAV-UV and SOIR at 120 km. The particle concentrations (cm^{-3}) are indicated.

We now evaluate the detectability at 220 nm of the clouds modelled in the previous section and the sensitivity of the results to the CO_2 uptake coefficient (γCO_2) and the MSP particle concentration. In the previous section γCO_2 was set equal to 0.1. Figure 10(a) illustrates the sensitivity of the cloud formation to γCO_2, for the atmospheric temperature/density profile from orbit 671.1 used previously, and with the MSP particle concentration fixed at 100 cm^{-3} between 110 km and 130 km. As expected, the peak particle size varies with γCO_2, for example when

517 γCO_2 is decreased by a factor of 100 from 0.1 to 10^{-3} the peak particle size only decreases by a
518 factor of ~10, and the peak height is essentially unchanged. This variation has consequences on
519 the detectability of the particles. Figure 10(b) shows the optical extinction at 220 nm of the cloud
520 as a function of γCO_2 for the same atmospheric profile. The Mie extinction is a strong function of
521 particle size, and so this cloud would be barely detectable (for the SPICAV-UV detection limit of
522 10^{-5} km^{-1}) if γCO_2 was less than 0.005.

523 In addition to the particle size, particle concentration plays a role in the detectability of the
524 clouds. In Figure 11 we test the sensitivity of the modelled cloud extinction to the assumed
525 number of MSP particles, with γCO_2 fixed at 0.1. In this case, the cloud would not be detectable
526 if the MSP number density fell below ~1 cm^{-3}. However, the MSP concentration is probably
527 much higher than this because a similar quantity of metal atoms is predicted to be injected via
528 meteoric ablation into the upper atmospheres of Venus and Earth (12.6 and 8.3 tonnes d^{-1},
529 respectively), and the MSP concentration in the terrestrial mesosphere above 75 km is around
530 2000 cm^{-3}, based on rocket-borne charge particle measurements and modelling (Plane et al.,
531 2014).

532 These sensitivity studies show that even if either the concentration of MSPs or the uptake
533 coefficient γCO_2 were a couple of orders of magnitude lower than for the standard model run, the
534 resulting CO_2-ice clouds would still be detectable. However, it is their very short lifetime of only
535 minutes, which would need to coincide with a satellite observation, which will make the
536 detection of these clouds challenging. The model results of (Listowski et al., 2014) revealed
537 similar short lifetimes for mesospheric CO_2 clouds on Mars that were dictated by the duration of
538 the supersaturated cold pockets. They concluded that the scarcity of cloud observations among
539 the hundreds of supersaturated temperature profiles observed by SPICAM was very probably due
540 to the short lifetimes (< 1 - 2 hours) of the cold pockets formed by upward propagating gravity
541 waves, and of the clouds themselves that rapidly evaporate in subsaturated conditions (10-20
542 minutes) (Listowski et al., 2014). If the cold pockets on Venus are a result of similar gravity
543 waves as on Mars, the cold pocket lifetime of 1-2 hours is a lower limit. According to our
544 simulations (see Figure 8) this cold pocket duration is sufficiently long for a detectable cloud to
545 form, sediment to a subsaturated environment and evaporate (< 20 minutes). Nevertheless, the
546 satellite observation would need to happen exactly at the right time and in the right place to be
547 able to catch these ephemeral clouds.

548

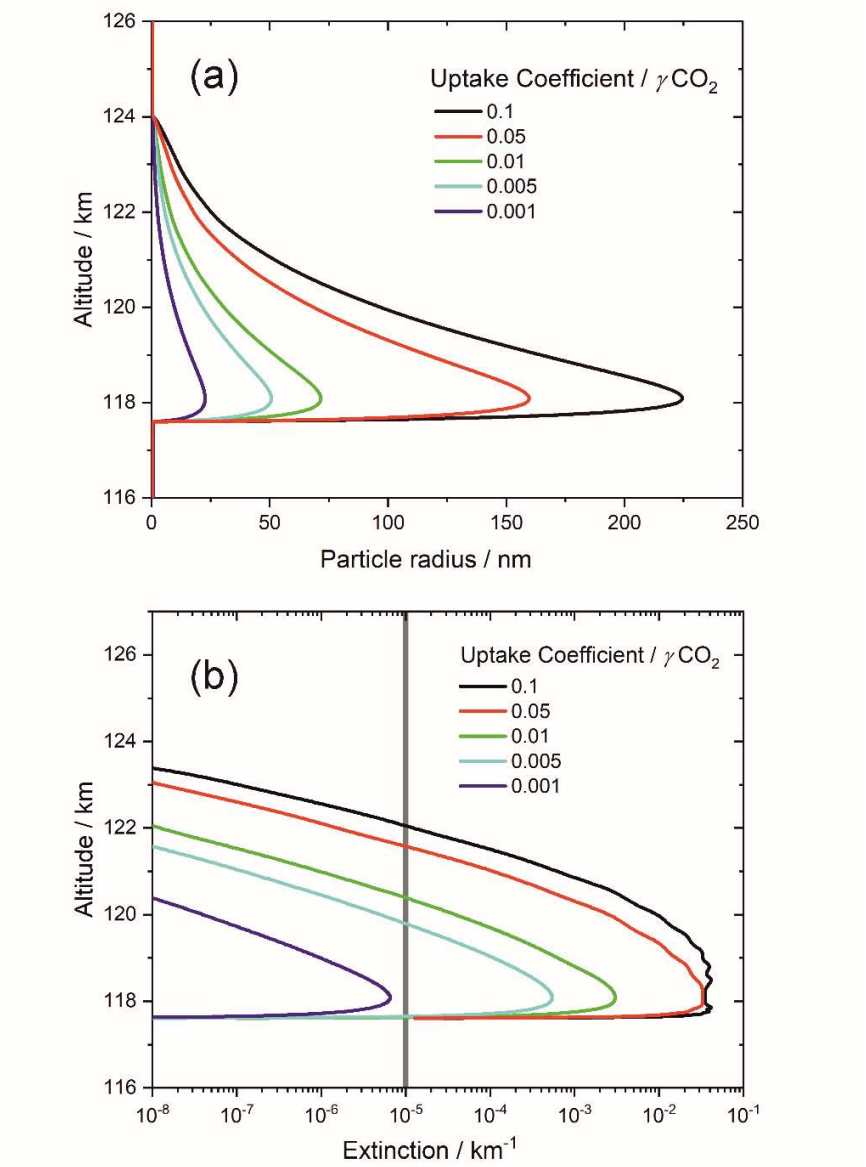

549

550 **Figure 7**. Sensitivity of (a) CO_2 ice particle growth, and (b) optical extinction at λ = 220 nm, to
551 the CO_2 uptake coefficient (γCO_2) for the conditions of orbit 671.1 (82.9° latitude) from Mahieux
552 et al. (2015). Number density of MSP particles = 100 cm^{-3}. The grey line in (b) shows the
553 detection limit (1×10^{-5} km^{-1}) of the SOIR instrument onboard Venus Express.

554

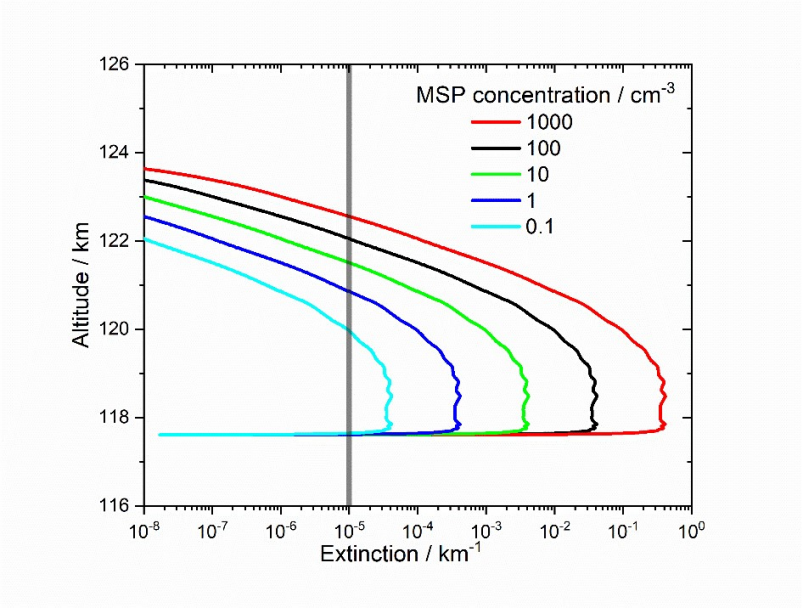

555

556 **Figure 8.** Extinction of CO_2 ice particles at λ = 220 nm, for a range of MSP particle
557 concentrations for the conditions of orbit 671.1 (γCO_2 = 0.1) from Mahieux et al. (2015). The
558 grey line shows the estimated detection limit of the SOIR instrument onboard Venus Express.

559

560 ## 3. Conclusions

561 The upper mesosphere of Venus between around 110 and 125 km is frequently cold
562 enough that the atmosphere is supersaturated with respect to both water and CO_2 ices. In fact, the
563 supersaturations become sufficiently large that both ASW H_2O ice and CO_2 ice can nucleate.
564 Based on a combination of classical and kinetic nucleation theory we propose that there is a
565 persistent ASW H_2O cloud layer on Venus around 10 km deep centered around 120 km. These
566 ASW particles may form both from heterogeneous nucleation on meteoric smoke particles, or
567 can form homogeneously directly from the vapour phase if the temperature minima persist for
568 longer than a few hours. The ASW cloud particles are unlikely to grow larger than ~5 nm given
569 the limited amount of water vapour present in the upper mesosphere of Venus. Hence, we
570 suggest that there is a persistent sub-visible layer of water ice particles, composed of ASW
571 covering around 50% of Venus at all latitudes. This 50% value is derived assuming the
572 terminator pressure and temperature measurements from SOIR are representative of other times
573 of the Venus day.

574 We also present evidence that CO_2 ice crystals can nucleate on either ASW particles or even bare
575 meteoric smoke particles. At latitudes greater than 60° (N and S) nucleation on ASW particles
576 can occur in more than 30% of the SOIR profiles. Since CO_2 is the primary component of
577 Venus' atmosphere, CO_2 particles will grow rapidly to 100s nm in only minutes. However,
578 these clouds will only have a lifetime of ~10-20 minutes since sedimentation is very rapid in the
579 thin upper mesosphere of Venus. These CO_2 ice particles are most likely composed of crystalline
580 CO_2 ice-I and will likely have a cubic, octahedral or cubo-octahedral shape (Mangan et al.,

2017b). These clouds may also produce halos that are unique to carbon dioxide crystals, as recently suggested for Mars (Ding et al., 2023). To an observer, VMCs might appear similar to *cirrus uncinus* (mares' tails) on Earth where nucleation occurs close to the temperature minimum, followed by sedimentation and growth and subsequent sublimation of the ice crystals as they fall into a subsaturated warmer region. Any wind shear would give the fall streaks curvature (*uncinus)*, where falling ice crystals are blown laterally as they sediment.

We have explored if VMCs might be observable with instruments on Venus Express. We find that the extinction will be large enough to observe at both 220 nm (SPICAV) and 3320 nm (SOIR), however the probability of an observation occurring in the 10-20 minutes that a cloud was present would be small. Nevertheless, we recommend that analysis of satellite date should be extended to altitudes where VMCs are predicted to occur, and that VMCs should be a target for future missions to Venus.

Given the strong sedimentation of VMC particles, VMCs have the potential to redistribute material in the upper atmosphere of Venus. Since nucleation of CO_2 on ASW with meteoric smoke cores is a likely mechanism for their production, VMCs are likely to transport MSPs to lower altitudes where they will be released in relatively narrow layers on the sublimation of CO_2 ice crystals. The formation of CO_2 crystals may also lead to the uptake of gas-phase meteoric species, which would also be released in a particulate form as the cloud particles sublimed at the base of the cloud layer (Mangan et al., 2017a). Similarly, VMCs will redistribute water vapour downwards, although the efficiency with which VMCs serve as a 'cold trap' will depend on the extent to which ASW particles can quench the supersaturation. On Earth, mesospheric clouds redistribute water downwards, resulting in a layer of enhanced water vapour at the base of the clouds, affecting odd oxygen and hydrogen chemistry (Murray & Plane, 2003; Murray & Plane, 2005). The extent to which VMCs limit the loss of water to space form Venus' atmosphere should be the subject of more detailed microphysical modelling constrained by observations.

Overall, this work reveals that there is a complex cloud system that forms in the upper mesosphere of Venus around much of the planet, involving both water and CO_2 ice particles. We predict a ubiquitous layer of nanoscale water ice particles that forms both homogeneously and heterogeneously and then provides the substrate on which CO_2 VMC particles can nucleate. The resulting crystals of CO_2 grow rapidly to sizes where they can fleetingly scatter light at a detectable level before sedimenting into a warmer layer where they sublime.

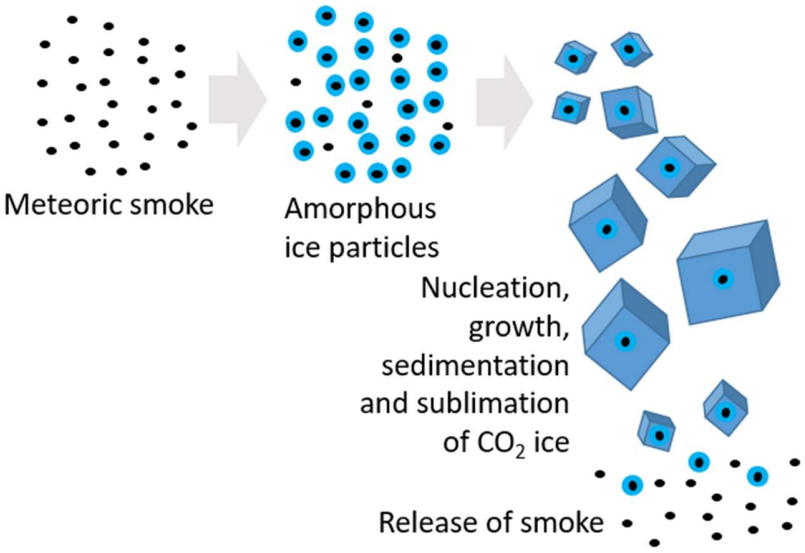

Figure 12. Formation and dissipation of Venusian mesospheric clouds. Meteoric smoke particles nucleate nanoscale amorphous ice particles, followed by the nucleation of CO_2 on those particles. The CO_2 crystals rapidly grow, probably with a cubic, octoheral or cubo-octohedral shape, then sediment and release the meteoric smoke particles as they sublime in a warmer part of the atmosphere.

Acknowledgments

This project was funded by the Science and Technology Facilities Council (STFC; ST/T000279/1). We thank Dr Arnaud Mahieux of the Belgian Institute for Space Aeronomy for providing the SOIR data we used in this paper.

Open Research

We have included all relevant equations and physical quantities to reproduce the plots in this paper in the appendicies.

Appendix A. Classical nucleation theory formalism

In this section we describe the nucleation theory we have applied to the atmosphere of Venus for both nucleation of CO_2 and H_2O phases and give the pertinent parameters in Table 1.

Homogeneous nucleation

The CNT formulation we have chosen to use for homogeneous nucleation is based on the equations set out in Määttänen et al. (2005). The free energy of formation of a spherical cluster of molecules with a radius r is described by

$$\Delta F_{\text{het}} = -\frac{4\pi r^3}{3\nu} kT \ln S + 4\pi r^2 \sigma \qquad \text{Eq. A1}$$

Where ν is the molecular volume of the condensed phase, σ is the interfacial energy between the condensed phase and the vapour phase, k the Boltzmann constant, T is temperature and S is the saturation ratio. A cluster is said to reach a critical size when the volume term (the left hand term) starts to dominate over the surface term (the right hand term). At the critical size further growth by addition of monomers results in an increase in stability, hence the critical cluster size and free energy of formation can be derived

$$r^* = \frac{2\nu\sigma}{kT \ln S} \qquad \Delta F^*_{\text{hom}} = \frac{16\pi\nu^2\sigma^3}{3(kT \ln S)^2} \qquad \text{Eq. A2}$$

The homogeneous nucleation rate is defined by an Arrhenius-like expression

$$J_{\text{hom}} = f_{\delta T} Z_{\text{hom}} \beta_{\text{hom}} c_{1,v} \exp\left(\frac{-\Delta F^*_{\text{hom}}}{kT}\right) \qquad \text{Eq. A3}$$

where $c_{1,v}$ is the concentration of monomers in the vapour phase. The dimensionless non-isothermal coefficient $f_{\delta T}$ as described in Feder et al. (1966) accounts for a reduction in the nucleation rate in cases when the atmospheric concentration of the nucleating species comprises a significant fraction of the total atmosphere. Higher collision frequency with the nucleating species compared to the inert carrier gas mean the heat of condensation is not efficiently removed from the cluster, leading to lower $f_{\delta T}$ values and therefore lower nucleation rates. In the case of water ice nucleation on Venus, given the low H_2O mixing ratio around 1 ppmv, the isothermal coefficient will be close to 1 and so have a minimal effect on the nucleation rate (Määttänen et al., 2005). Using the lowest value of 0.966 reported by Määttänen et al. (2005) for H_2O in the comparable case of Mars, increases the nucleation activation temperature by < 0.1 K. Using the lowest non-isothermal value of 0.006 reported for CO_2 ice nucleation (also for Mars) from (Wood, 1999), still only causes an approximate 0.3 K increase .

Z_{hom} is the homogeneous Zeldovich factor that accounts for the decrease in rate of cluster formation when there is a finite rate of critical cluster formation and is define as

$$Z_{\text{hom}} = \sqrt{\frac{\Delta F^*_{\text{hom}}}{3\pi k \quad ^{*2}}} \qquad \text{Eq. A4}$$

Where n^* is the number of molecules in the critical cluster. β_{hom} describes the rate at which momomers collide with the cluster and is defined as

$$\beta_{\mathrm{hom}} = c_{1,v} 4\pi r^{*2} \sqrt{\frac{kT}{2\pi m_{\mathrm{m}}}} \quad \text{Eq. A5}$$

where m_{m} is the molar mass.

Heterogeneous nucleation

The rate of heterogeneous nucleation induced via surface diffusion on a spherical nucleus (J_{het}, a per nucleating particle nucleation rate in units of s^{-1}), is given by:

$$J_{het} = A_{\mathrm{N}} f_{\delta T} Z_{\mathrm{het}} \beta_{\mathrm{het}} c_{1,s} \exp\left(\frac{-\Delta F^*_{\mathrm{het}}}{kT}\right) \quad \text{Eq. A6}$$

where A_{N} is the surface area of the ice nucleating particle and $c_{1,s}$ is the concentration of monomers on the particle surface; β_{het} describes the diffusion of molecules on the particle surface, and the dissociation of a proportion of supercritical clusters is described by the heterogeneous Zeldovich factor Z_{het}. ΔF_{het} is the free energy of forming a critical cluster on the nucleating particle, given by:

$$\Delta F^*_{\mathrm{het}} = f(m,x) \frac{16\pi\sigma^3 v^2}{3(kT\ln\ )^2} \quad \text{Eq. A7}$$

$\Delta F^*_{\mathrm{het}}$ is calculated relative to the homogeneous barrier ($\Delta F^*_{\mathrm{hom}}$) with a reduction in the energy barrier by a factor $f(m,x)$ as described in Fletcher (1958), where x is the ratio of the size of the nucleating particle to the size of the critical cluster and m is the contact parameter (equal to $\cos\theta$, where θ is the contact angle between the ice nucleating particle and the nucleating phase (pertinent values of θ are discussed in the following section).

Table 1. Physical properties of H_2O and CO_2

Property	Value	Notes
ASW		
Saturation vapour pressure	$P_{\mathrm{sat,hex}} = \exp\left(\frac{2312 - 1.6T}{RT}\right)$	(Nachbar et al., 2018)
Density	940 kg m^{-3}	(Ghormley & Hochanadel, 1971)

Surface tension	0.085 J m^{-2}	Derived from (Duft et al., 2019, pp. author-year)
Desorption energy on MSP	42 kJ mol^{-1}	(Duft et al., 2019)
Vibrational frequency	10^{13} s^{-1}	(Pruppacher & Klett, 1997)
Mean jump distance	0.32 nm	(Pruppacher & Klett, 1997)
Contact parameter on MSP	0.999	Duft et al. (2019) suggest $m = 1$
Ice I_h		
Saturation vapour pressure	$\exp(9.550426 - 5723.265/T + 3.53068 \ln(T) - 0.00728332T)$ (Pa)	(Murphy & Koop, 2005)
Density	$(-1.3103 \cdot 10^{-0} \cdot T^3 + 3.8109 \cdot 10^{-7} \cdot T^2 - 9.2592 \cdot 10^{-5} \cdot T + 0.94040) \cdot 1000$ (kg m^{-3})	(Murray & Jensen, 2010)
Surface tension	$0.141 - 0.00015T$ (J m^{-2})	(Hale & Plummer, 1974)
Desorption energy	17.5 kJ mol^{-1}	(Seki & Hasegawa, 1983)
Vibrational frequency	10^{13} s^{-1}	(Määttänen et al., 2005)
Mean jump distance	0.32 nm	(Pruppacher & Klett, 1997)
Contact parameter on MSP	0.985	(Saunders et al., 2010)
CO_2 crystal		
Saturation vapour pressure	$1.38 \cdot 10^{12} \exp(-3182.48/T)$ (Pa)	(Azreg-Aïnou, 2005)
Density	$1.72391 - 0.000253T - 0.00000287T^2$ (g cm^{-3})	(Mangan et al., 2017b)
Surface tension	0.08 (J m^{-2})	(Nachbar et al., 2016; Wood, 1999)
Desorption energy	18.5 kJ mol^{-1}	(Nachbar et al., 2016)
Vibrational frequency	$2.9 \cdot 10^{12}$ s^{-1}	(Nachbar et al., 2016)
Mean jump distance	0.4 nm	(Nachbar et al., 2016; Wood, 1999)
Contact parameter on ice	0.95	(Glandorf et al., 2002)

Contact parameter on MSP	0.78	(Nachbar et al., 2016)
CO_2 liquid		
Saturation vapour pressure	$=101325 \cdot 10^{-A}$ $A = 1353/T - 8.143 \cdot \log(T) + 0.006259 \cdot T + 24.619$	(Dingilian et al., 2020; Michels et al., 1950)
Density	$\ln\left(\frac{\rho'}{\rho_c}\right) = \sum_{i=1}^{4} a_i \left(1 - \frac{T}{T_c}\right)^{t_i}$ $a_1 = 1.9245108$; $a_2 = -0.62385555$; $a_3 = -0.32731127$; $a_4 = 0.39245142$; $t_1 = 0.34$; $t_2 = 0.5$; $t_3 = 10/6$; $t_4 = 11/6$; $T_c = 304.1282$; $\rho_c = 467.6$ kg m^{-3}	(Dingilian et al., 2020; Span & Wagner, 1996)
Surface tension	0.0378 J m^{-2}	Derived from fit to data in Dingilian et al. (2020), see text.

Notes on the choice and derivation of physical properties of condensed phases of H_2O and CO_2

There are significant uncertainties associated with the physical properties of CO_2 and H_2O under the extremely low temperatures in Venus's upper atmosphere. Hence, any predictions with CNT need to be taken in the context of these large uncertainties that propagate through into the nucleation rate. For the CNT formulations in this paper we have used a combination of physical properties used in previous nucleation studies and values derived from recent experimental data. The physical properties used in this study are detailed in Table 1. In the cases where physical properties were derived or there was a choice, the methodology and discussion is given below.

Amorphous solid water: The homogeneous nucleation of amorphous solid water was determined assuming a water mixing ratio of 1 ppm and the saturation vapour pressure was defined by (Nachbar et al., 2019) and Nachbar et al. (2018). In the past the parameterisation for the saturation pressure from (Murphy & Koop, 2005), where ASW and supercooled water were assumed to be a single continuous phase, was been used. However (Nachbar et al., 2019) show that ASW and supercooled water are two distinct phases of water and have distinct thermodynamics. Nachbar et al. (2018) showed that the vapour pressure of ASW is substantially greater than that predicted by the parameterisation given by (Murphy & Koop, 2005). Surface tension of ASW is not directly measured in the literature, and we used a value that we derived from literature data for the adsorption of ASW on MSPs (Duft et al., 2019); we discuss this

derivation in the heterogeneous section below. We set the non-isothermal constant to unity, which is probably an overestimate, but since we are attempting to identify which mechanisms are possible introducing a highly uncertain term that would reduce the rate would not be helpful.

Using a two-structure model of water (Hruby & Holten, 2004) produce a surface tension value of ~0.095 Jm^{-2} for water in the temperature regime associated with Venus' upper mesosphere. Interestingly, they suggest that the temperature dependence of this value below ~120 K is weak. In a study where adsorption of ASW onto MSP particles was studied between 128 and 147 K (Duft et al., 2019) found that the surface tension was 0.094 ±0.011 J m^{-2}. In order to derive a surface tension that was consistent with our CNT formulation we fitted to the data presented in (Duft et al., 2019). They report critical supersaturations where adsorption of water led to ice-activation. We interpreted the saturation at which we see a step change in the nucleation rate as being equivalent to the critical supersaturation reported by (Duft et al., 2019). The nucleation rate is very sensitive to the desorption energy and we have used an average value of 42 kJ mol^{-1} which is in the range reported by (Duft et al., 2019) for different MSP materials. This desorption energy is somewhat larger than used by (Määttänen et al., 2005) and reflects the strong binding of water molecules to the polar MSP surface. Given the critical cluster is only a few 10s of molecules in size, the assumption that all these molecules experience an enhanced interaction with the surface is reasonable (Duft et al., 2019). We also follow (Duft et al., 2019) in assuming that the MSP is wetted by ASW with *m* of 0.999. We fitted to reproduce the critical supersaturations in their Fig 6, yielding a surface tension of 0.085 J m^{-2}, which is within the uncertainty of the values reported by (Duft et al., 2019). By constraining our CNT formulation to experimental data down to 120 K, we can have some confidence in the extrapolation to ~110 K where we predict nucleation in Venus' atmosphere.

Liquid CO_2. It is not immediately obvious that liquid CO_2 should play any role in the atmosphere of Venus since bulk liquid CO_2 can only exist at much greater pressures. However, recent experiments and computational studies have demonstrated that the initial cluster to form via homogeneous nucleation has liquid-like properties at temperatures pertinent to the upper atmosphere of Venus (Dingilian et al., 2020) (Halonen et al., 2021). In order to produce a CNT formulation that is consistent with the nucleation rate (and supersaturation) data presented in (Dingilian et al., 2020) we fitted the surface tension to the nucleation rate data between 78 K and 92 K. The average was 0.0378 ± 0.0014 J m^{-2}. (Dingilian et al., 2020) fitted their data using a parameterisation for surface tension based on high-temperature data, that was then extrapolated to the low temperatures of their experiments, producing values of 0.050 to 0.054 J m^{-2}. While there are uncertainties in these physical quantities, the pairing of the surface tension with our formulation of CNT to reproduce the experimentally observed nucleation rates under conditions close to those where clouds may form in Venus' upper mesosphere gives us some confidence in our results.

Appendix B: Rate coefficients for attachment and detachment of CO_2 molecules to $MgCO_3(CO_2)_n$ clusters

Rate coefficients for the sequential addition of CO_2 molecules to $MgCO_3(CO_2)_3$, up to $MgCO_3(CO_2)_{40}$, were calculated with Rice Ramsperger Kassel Markus (RRKM) theory, using a

746 solution of the Master Equation based on the inverse Laplace transform method (De Avillez
747 Pereira et al., 1997). These $MgCO_3(CO_2)_n + CO_2$ recombination reactions proceed via the
748 formation of an excited adduct, which can either dissociate back to reactants or be stabilized by
749 collision with a third body to form $MgCO_3(CO_2)_{n+1}$. The binding energy of each CO_2 to the
750 cluster was fixed to 26.6 kJ mol^{-1}, which is the heat of sublimation of CO_2 at 0 K (Chicko, 2022;
751 Giauque & Egan, 1937). The internal energy of the adduct was divided into a contiguous set of
752 grains with a width of 12 cm^{-1} (which reflects the small binding energy of CO_2 to the cluster),
753 each containing a bundle of rovibrational states.

754 The density of states of the adduct was calculated using the Beyer − Swinehart algorithm (Gilbert
755 & Smith, 1990) for the vibrational modes (without making a correction for anharmonicity). For
756 each $MgCO_3(CO_2)_n$ cluster these modes were taken to consist of the vibrational modes of
757 $MgCO_3$ (167, 490, 530, 673, 806, 826, 903, 990, 1768 cm^{-1}) and the n CO_2 ligands (676, 676,
758 1364, 2400 cm^{-1} for each CO_2), calculated at the B3LYP/6-311+g(2d,p) level of theory (Frisch et
759 al., 2016) and assumed to be independent of each other; and a further 5n low-frequency modes
760 set to a frequency of 80 cm^{-1}. This frequency represents the geometric mean of the frequencies
761 of the "new" vibrational modes that are created when n CO_2 molecules cluster with $MgCO_3$. The
762 actual geometric means for n = 2, 3 and 4 are 75.1, 83.2 and 78.5 cm^{-1}, respectively, using the
763 data in Table S3 in the SI of Plane et al. (2018). The geometric mean is used because the density
764 of states of the cluster is proportional to the inverse product of the vibrational frequencies
765 (Gilbert & Smith, 1990). A classical densities of states treatment was used for the rotational
766 modes. Since the clusters will be approximately spherical as they grow, the moments of inertia
767 were approximated to be that of a solid sphere about its diameter:

768 $$I = 0.4Mr^2$$
769 Eq. B1

770 where M is the mass of the cluster, and r is the cluster radius assuming a density of 1562 kg m^{-3}
771 for solid CO_2 at 195 K.

772 Each grain associated with the adduct $MgCO_3(CO_2)_{n+1}$ was then assigned a set of microcanonical
773 rate coefficients for dissociation back to $MgCO_3(CO_2)_n + CO_2$. These rate coefficients are
774 determined using inverse Laplace transformation to link them directly to $k_{rec,\infty}$, which is
775 estimated here as the hard sphere collision frequency between $MgCO_3(CO_2)_n$ and CO_2, with a
776 small $T^{1/2}$ temperature dependence (Smith, 1980). The probability of collisional transfer between
777 grains was estimated using the exponential down model, where the average energy for downward
778 transitions $\langle \Delta E \rangle_{down}$ was set to 600 cm^{-1} which is typical of M = CO_2 at 300 K, and treated as
779 independent of temperature (Gilbert & Smith, 1990). The Master Equation, which describes the
780 evolution with time of the grain populations of the adduct, was then expressed in matrix form
781 and solved to yield the rate coefficients for sequential addition of CO_2 to the clusters, as a
782 function of temperature (50 – 150 K) at a pressure of 10^{-5} Torr, which is the typical pressure at
783 ~150 km in Venus' atmosphere (Mahieux et al., 2015).

784 For the purpose of atmospheric modelling, it is customary to use the uptake coefficient, γ. This
785 was calculated as ratio of the recombination rate coefficient to the collision rate of CO_2 with a
786 sphere of radius r:

$$\gamma = \frac{k_{rec}[\mathrm{CO_2}]}{(0.25\bar{c}A)} \quad \text{Eq. B2}$$

where k_{rec} is the recombination rate coefficient, $\bar{c}$ is the mean collision speed between $MgCO_3(CO_2)_n$ and CO_2, and A is the surface area of the cluster ($4\pi r^2$). γ is illustrated as a function of n and T in Figure B1(a). Note that γ does not exceed unity, which is a good test of the Master Equation calculation.

Finally, the rate of dissociation of the cluster i.e. $MgCO_3(CO_2)_{n+1} \rightarrow MgCO_3(CO_2)_n + CO_2$, was calculated by detailed balance with the recombination rate coefficient, where the equilibrium constant is calculated by statistical mechanics with the partition functions for $MgCO_3(CO_2)_{n+1}$ and $MgCO_3(CO_2)_n$ using the vibrational frequencies and rotational constants described above. The equilibrium constant is within 20% of that given by the Antoine relation (Chicko, 2022; Giauque & Egan, 1937) for clusters larger than $n = 30$ and $T > 140$ K (where the Antoine relation is valid). The dissociation rate, i.e., the evaporation rate, is shown as a function of n and T in Figure B1b.

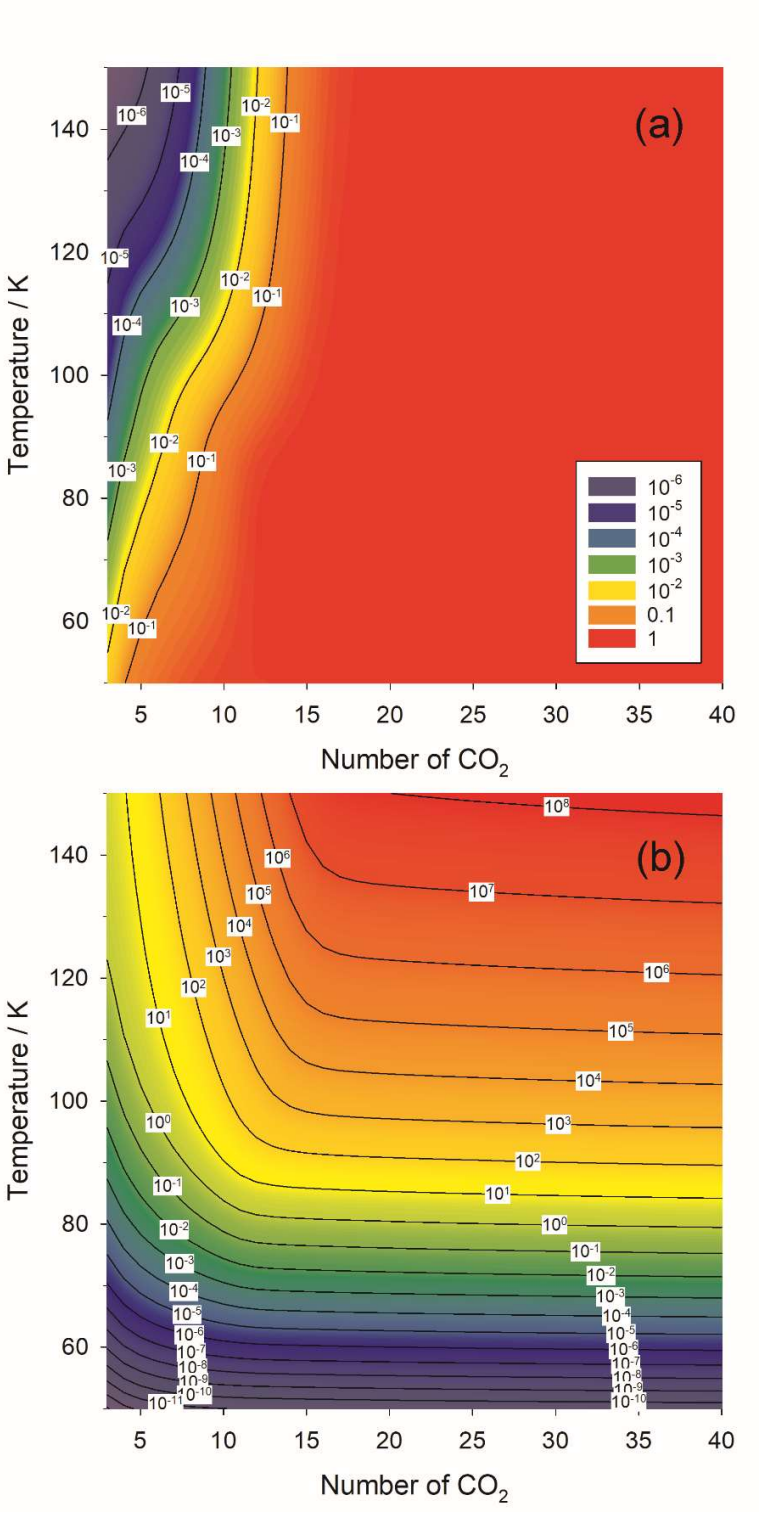

Figure B1. (a) γCO_2 as a function of temperature and number of CO_2 molecules clustered around a meteoric smoke particle. (b) Rate of evaporation (units: molecule s^{-1}) of CO_2 from an MSP-$(CO_2)_n$ cluster, as a function of temperature and the number of CO_2 molecules (n).

Appendix C: Details of the microphysical model

In order to explore the evolution of the CO_2-ice clouds, a 1-dimensional model was constructed which describes the nucleation, growth, sedimentation and sublimation of the ice particles. For this simple cloud model we describe the production of CO_2 particles using the KNT theory presented in section 2.4. Hence, we implicitly assume that nucleation occurs on MSP, probably $MgCO_3$ and $FeCO_3$. Although we expect very similar results in terms of growth, sedimentation and lifetime of cloud particles if nucleation occurred on ASW particles which in turn nucleated on MSPs.

When the concentration of MSPs is larger than ~ 1000 cm^{-3}, the production of large CO_2 particles with radii of a few hundred nm starts to deplete significantly the background CO_2 density (this effect is accounted for in the model). Because the CO_2 ice clouds are short-lived, coagulation of ice particles is neglected.

The sedimentation velocity of the $MgCO_3(CO_2)_n$ clusters and CO_2 ice particles, w_i, can be estimated using a form of Stokes' law describing a spherical particle falling through a stationary fluid :

$$w_i = \frac{2(\rho_p - \rho_{air})}{9\mu} g\, r_i^2 C_{scf} \qquad \text{Eq. C1}$$

where ρ_p and ρ_{air} are the particle density (taken to be the density for solid CO_2, which is 1562 kg m^{-3} at 195 K) and the air density, respectively; μ is the dynamic viscosity of CO_2 at the atmospheric temperature and pressure; g is the gravitational constant (8.87 m s^{-2} for Venus); and r_i is the particle radius. C_{scf} is the Cunningham slip correction factor accounting for the effects of drag on small particles, and is estimated from equation Eq.B2, where λ is the mean free path of the CO_2 molecules, and A_1, A_2 and A_3 are dimensionless coefficients :

$$C_{scf} = 1 + \frac{\lambda}{r_i}\left(A_1 + A_2 exp\left(\frac{-A_3 r_i}{\lambda}\right)\right) \qquad \text{Eq. C2}$$

References

Azreg-Aïnou, M. (2005). Low-temperature Data for Carbon Dioxide. *Monatshefte für Chemie*, *136*(12), 2017-2027. https://doi.org/10.1007/s00706-005-0370-3

Bottema, M., Plummer, W., Strong, J., & Zander, R. (1965). The composition of the Venus clouds and implications for model atmospheres. *70*(17), 4401-4402. https://doi.org/10.1029/JZ070i017p04401

Bromley, S. T., Gómez Martín, J. C., & Plane, J. M. C. (2016). Under what conditions does (SiO)N nucleation occur? A bottom-up kinetic modelling evaluation [10.1039/C6CP03629E].

838 *Physical Chemistry Chemical Physics*, *18*(38), 26913-26922.
839 https://doi.org/10.1039/C6CP03629E

840 Carrillo-Sánchez, J. D., Gómez-Martín, J. C., Bones, D. L., Nesvorný, D., Pokorný, P., Benna, M.,
841 Flynn, G. J., & Plane, J. M. C. (2020). Cosmic dust fluxes in the atmospheres of Earth,
842 Mars, and Venus. *Icarus*, *335*, 113395.
843 https://doi.org/https://doi.org/10.1016/j.icarus.2019.113395

844 Chamberlain, S., Mahieux, A., Robert, S., Piccialli, A., Trompet, L., Vandaele, A. C., & Wilquet,
845 V. (2020). SOIR/VEx observations of water vapor at the terminator in the Venus
846 mesosphere. *Icarus*, *346*, 113819. https://doi.org/10.1016/j.icarus.2020.113819

847 Chicko, J. S. (2022). Heat of Sublimation Data. In P. J. Linstrom & W. G. Mallard (Eds.), *NIST*
848 *Chemistry WebBook, NIST Standard Reference Database Number 69*. Gaithersburg MD,
849 20899: National Institute of Standards and Technology.

850 De Avillez Pereira, R., Baulch, D. L., Pilling, M. J., Robertson, S. H., & Zeng, G. (1997).
851 Temperature and Pressure Dependence of the Multichannel Rate Coefficients for the CH_3+
852 OH System. *J. Phys. Chem.*, *101*, 9681-9693.

853 Ding, J., Yang, P., Lemmon, M. T., & Zhang, Y. (2023). Simulations of Halos Produced by Carbon
854 Dioxide Ice Crystals in the Martian Atmosphere [https://doi.org/10.1029/2023GL103457].
855 *Geophysical Research Letters*, *50*(8), e2023GL103457.
856 https://doi.org/https://doi.org/10.1029/2023GL103457

857 Dingilian, K. K., Halonen, R., Tikkanen, V., Reischl, B., Vehkamäki, H., & Wyslouzil, B. E.
858 (2020). Homogeneous nucleation of carbon dioxide in supersonic nozzles I: experiments
859 and classical theories [10.1039/D0CP02279A]. *Physical Chemistry Chemical Physics*,
860 *22*(34), 19282-19298. https://doi.org/10.1039/D0CP02279A

861 Duft, D., Nachbar, M., & Leisner, T. (2019). Unravelling the microphysics of polar mesospheric
862 cloud formation. *Atmos. Chem. Phys.*, *19*(5), 2871-2879. https://doi.org/10.5194/acp-19-
863 2871-2019

864 Feder, J., Russell, K. C., Lothe, J., & Pound, G. M. (1966). Homogeneous nucleation and growth
865 of droplets in vapours. *Advances in Physics*, *15*(57), 111-178.
866 https://doi.org/10.1080/00018736600101264

867 Fedorova, A. A., Montmessin, F., Korablev, O., Luginin, M., Trokhimovskiy, A., Belyaev, D. A.,
868 Ignatiev, N. I., Lefèvre, F., Alday, J., Irwin, P. G. J., Olsen, K. S., Bertaux, J.-L., Millour,
869 E., Määttänen, A., Shakun, A., Grigoriev, A. V., Patrakeev, A., Korsa, S., Kokonkov, N., .
870 . . Wilson, C. F. (2020). Stormy water on Mars: The distribution and saturation of
871 atmospheric water during the dusty season. *Science*, *367*(6475), 297-300.
872 https://doi.org/10.1126/science.aay9522

873 Fletcher, N. H. (1958). Size effect in heterogeneous nucleation. *The Journal of Chemical Physics*,
874 *29*(3), 572-576. https://doi.org/doi:http://dx.doi.org/10.1063/1.1744540

875 Frisch, M. J., Trucks, G. W., Schlegel, H. B., Scuseria, G. E., Robb, M. A., Cheeseman, J. R.,
876 Scalmani, G., Barone, V., Petersson, G. A., Nakatsuji, H., Li, X., Caricato, M., Marenich,
877 A. V., Bloino, J., Janesko, B. G., Gomperts, R., Mennucci, B., Hratchian, H. P., Ortiz, J.
878 V., . . . Fox, D. J. (2016). *Gaussian 16, Revision B.01*. In Gaussian, Inc.

879 Ghormley, J. A., & Hochanadel, C. J. (1971). Amorphous ice: density and reflectivity. *Science*,
880 *171*(3966), 62-64. https://doi.org/10.1126/science.171.3966.62

881 Giauque, W. F., & Egan, C. J. (1937). Carbon Dioxide. The Heat Capacity and Vapor Pressure of
882 the Solid. The Heat of Sublimation. Thermodynamic and Spectroscopic Values of the
883 Entropy. *J. Chem. Phys.*, *5*, 45-54. https://doi.org/ https://doi.org/10.1063/1.1749929

884 Gilbert, R. G., & Smith, S. C. (1990). *Theory of Unimolecular and Recombination Reactions*.
885 Blackwell.

886 Glandorf, D. L., Colaprete, A., Tolbert, M. A., & Toon, O. B. (2002). CO_2 snow on Mars and early
887 Earth: Experimental constraints. *Icarus*, *160*(1), 66-72.
888 https://doi.org/10.1006/icar.2002.6953

889 Hale, B. N., & Plummer, P. L. M. (1974). On Nucleation Phenomena I: A Molecular Model.
890 *Journal of Atmospheric Sciences*, *31*(6), 1615-1621. https://doi.org/10.1175/1520-
891 0469(1974)031<1615:ONPIAM>2.0.CO;2

892 Halonen, R., Tikkanen, V., Reischl, B., Dingilian, K. K., Wyslouzil, B. E., & Vehkamäki, H.
893 (2021). Homogeneous nucleation of carbon dioxide in supersonic nozzles II: molecular
894 dynamics simulations and properties of nucleating clusters. *Physical Chemistry Chemical*
895 *Physics*, *23*(8), 4517-4529. https://doi.org/10.1039/D0CP05653G

896 Hervig, M. E., Plane, J. M. C., Siskind, D. E., Feng, W., Bardeen, C. G., & Bailey, S. M. (2021).
897 New Global Meteoric Smoke Observations From SOFIE: Insight Regarding Chemical
898 Composition, Meteoric Influx, and Hemispheric Asymmetry. *J. Geophys. Res.-Atmos.*,
899 *126*, art. no.: e2021JD035007. https://doi.org/10.1029/2021jd035007

900 Hruby, J., & Holten, V. (2004). *A two-structure model of thermodynamic properties and surface*
901 *tension of supervooled water* Proceedings of the 14th International Conference on the
902 Properties of Water and Steam, Maruzen.

903 Kofman, V., He, J., Loes ten Kate, I., & Linnartz, H. (2019). The Refractive Index of Amorphous
904 and Crystalline Water Ice in the UV–vis. *The Astrophysical Journal*, *875*(2), 131.
905 https://doi.org/10.3847/1538-4357/ab0d89

906 Listowski, C., Määttänen, A., Montmessin, F., Spiga, A., & Lefevre, F. (2014). Modeling the
907 microphysics of CO_2 ice clouds within wave-induced cold pockets in the martian
908 mesosphere. *Icarus*, *237*, 239-261. https://doi.org/10.1016/j.icarus.2014.04.022

909 Listowski, C., Määttänen, A., Riipinen, I., Montmessin, F., & Lefevre, F. (2013). Near-pure vapor
910 condensation in the Martian atmosphere: CO_2 ice crystal growth. *Journal of Geophysical*
911 *Research-Planets*, *118*(10), 2153-2171. https://doi.org/10.1002/jgre.20149

912 Lübken, F. J., Lautenbach, J., Höffner, J., Rapp, M., & Zecha, M. (2009). First continuous
913 temperature measurements within polar mesosphere summer echoes. *Journal of*
914 *Atmospheric and Solar-Terrestrial Physics*, *71*(3–4), 453-463.
915 https://doi.org/http://dx.doi.org/10.1016/j.jastp.2008.06.001

916 Luginin, M., Fedorova, A., Belyaev, D., Montmessin, F., Wilquet, V., Korablev, O., Bertaux, J.
917 L., & Vandaele, A. C. (2016). Aerosol properties in the upper haze of Venus from SPICAV
918 IR data. *Icarus*, *277*, 154-170. https://doi.org/https://doi.org/10.1016/j.icarus.2016.05.008

919 Määttänen, A., Vehkamaki, H., Lauri, A., Merikallio, S., Kauhanen, J., Savijarvi, H., & Kulmala,
920 M. (2005). Nucleation studies in the Martian atmosphere. *Journal of Geophysical*
921 *Research-Planets*, *110*(E2). https://doi.org/10.1029/2004je002308

922 Määttänen, A., Vehkamaki, H., Lauri, A., Napari, I., & Kulmala, M. (2007). Two-component
923 heterogeneous nucleation kinetics and an application to Mars. *Journal of Chemical*
924 *Physics*, *127*(13). https://doi.org/10.1063/1.2770737

925 Mahieux, A., Vandaele, A. C., Bougher, S. W., Drummond, R., Robert, S., Wilquet, V.,
926 Chamberlain, S., Piccialli, A., Montmessin, F., Tellmann, S., Pätzold, M., Häusler, B., &
927 Bertaux, J. L. (2015). Update of the Venus density and temperature profiles at high altitude
928 measured by SOIR on board Venus Express. *Planetary and Space Science*, *113-114*, 309-
929 320. https://doi.org/10.1016/j.pss.2015.02.002

930 Mangan, T. P., Frankland, V. L., Murray, B. J., & Plane, J. M. C. (2017a). The fate of meteoric
931 metals in ice particles: Effects of sublimation and energetic particle bombardment. *Journal*
932 *of Atmospheric and Solar-Terrestrial Physics*, *161*, 143-149.
933 https://doi.org/https://doi.org/10.1016/j.jastp.2017.07.002

934 Mangan, T. P., Plane, J. M. C., & Murray, B. J. (2021). The Phase of Water Ice Which Forms in
935 Cold Clouds in the Mesospheres of Mars, Venus, and Earth. *Journal of Geophysical*
936 *Research: Planets*, *126*(3), e2020JE006796. https://doi.org/10.1029/2020JE006796

937 Mangan, T. P., Salzmann, C. G., Plane, J. M. C., & Murray, B. J. (2017b). CO2 ice structure and
938 density under Martian atmospheric conditions. *Icarus*, *294*, 201-208.
939 https://doi.org/10.1016/j.icarus.2017.03.012

940 Menzel, D. H., & Whipple, F. L. J. T. A. J. (1954). The case for H2O clouds on Venus. *59*, 329.
941 https://doi.org/10.1086/107037

942 Michels, A., Wassenaar, T., Zwietering, T., & Smits, P. (1950). The vapour pressure of liquid
943 carbon dioxide. *Physica*, *16*(5), 501-504. https://doi.org/https://doi.org/10.1016/0031-
944 8914(50)90135-2

945 Montmessin, F., Bertaux, J.-L., Quémerais, E., Korablev, O., Rannou, P., Forget, F., Perrier, S.,
946 Fussen, D., Lebonnois, S., Rébérac, A., & Dimarellis, E. (2006). Subvisible CO2 ice clouds
947 detected in the mesosphere of Mars. *Icarus*, *183*(2), 403-410.
948 https://doi.org/https://doi.org/10.1016/j.icarus.2006.03.015

949 Mullin, J. W. (2001). *Crystallization*. Elsevier.

950 Murphy, D. M., & Koop, T. (2005). Review of the vapour pressures of ice and supercooled water
951 for atmospheric applications. *Q.J.R. Meteorol. Soc.*, *131*(608), 1539-1565.
952 https://doi.org/10.1256/qj.04.94

953 Murray, B. J., & Jensen, E. J. (2010). Homogeneous nucleation of amorphous solid water particles
954 in the upper mesosphere. *Journal of Atmospheric and Solar-Terrestrial Physics*, *72*(1), 51-
955 61. https://doi.org/https://doi.org/10.1016/j.jastp.2009.10.007

956 Murray, B. J., & Plane, J. M. C. (2003). The uptake of atomic oxygen on ice films: Implications
957 for noctilucent clouds [10.1039/B305555H]. *Physical Chemistry Chemical Physics*, *5*(19),
958 4129-4138. https://doi.org/10.1039/B305555H

959 Murray, B. J., & Plane, J. M. C. (2005). Modelling the impact of noctilucent cloud formation on
960 atomic oxygen and other minor constituents of the summer mesosphere. *Atmospheric*
961 *Chemistry and Physics*, *5*, 1027-1038. <Go to ISI>://000227997600002

962 Nachbar, M., Duft, D., & Leisner, T. (2018). The vapor pressure over nano-crystalline ice. *Atmos.*
963 *Chem. Phys.*, *18*(5), 3419-3431. https://doi.org/10.5194/acp-18-3419-2018

964 Nachbar, M., Duft, D., & Leisner, T. (2019). The vapor pressure of liquid and solid water phases
965 at conditions relevant to the atmosphere. *J. Chem. Phys.*, *151*(6), 064504.
966 https://doi.org/10.1063/1.5100364

967 Nachbar, M., Duft, D., Mangan, T. P., Martin, J. C. G., Plane, J. M. C., & Leisner, T. (2016).
968 Laboratory measurements of heterogeneous CO_2 ice nucleation on nanoparticles under
969 conditions relevant to the Martian mesosphere. *Journal of Geophysical Research Planets*,
970 *121*, 753 - 769. https://doi.org/10.1002/2015JE004978

971 Palen, S., Kay, L., Smith, B., & Blumenthal, G. (2019). *Understanding our universe* (3rd ed.). W.
972 W. Norton & Co.

973 Plane, J. M. C., Carrillo-Sanchez, J. D., Mangan, T. P., Crismani, M. M. J., Schneider, N. M., &
974 Määttänen, A. (2018). Meteoric Metal Chemistry in the Martian Atmosphere. *Journal of*
975 *Geophysical Research Planets*, *123*(3), 695-707. https://doi.org/10.1002/2017je005510

976 Plane, J. M. C., Feng, W., & Dawkins, E. C. M. (2015). The Mesosphere and Metals: Chemistry
977 and Changes. *Chemical Reviews*, *115*(10), 4497-4541. https://doi.org/10.1021/cr500501m

978 Plane, J. M. C., Saunders, R. W., Hedin, J., Stegman, J., Khaplanov, M., Gumbel, J., Lynch, K.
979 A., Bracikowski, P. J., Gelinas, L. J., Friedrich, M., Blindheim, S., Gausa, M., & Williams,
980 B. P. (2014). A combined rocket-borne and ground-based study of the sodium layer and
981 charged dust in the upper mesosphere. *J. Atmos. Solar-Terr. Phys.*, *118*, 151–160.

982 Pollack, J. B., & Sagan, C. (1968). The case for ice clouds on Venus. *73*(18), 5943-5949.
983 https://doi.org/10.1029/JB073i018p05943

984 Pruppacher, H. R., & Klett, J. D. (1997). *Microphysics of clouds and precipitation*. Kluwer
985 Academic Publishers. http://site.ebrary.com/id/10067306

986 Rea, D. G., & O'Leary, B. T. (1968). On the composition of the Venus clouds. *73*(2), 665-675.
987 https://doi.org/10.1029/JB073i002p00665

988 Saunders, R. W., Möhler, O., Schnaiter, M., Benz, S., Wagner, R., Saathoff, H., Connolly, P. J.,
989 Burgess, R., Murray, B. J., Gallagher, M., Wills, R., & Plane, J. M. C. (2010). An aerosol
990 chamber investigation of the heterogeneous ice nucleating potential of refractory
991 nanoparticles. *Atmos. Chem. Phys.*, *10*(3), 1227-1247. https://doi.org/10.5194/acp-10-
992 1227-2010

993 Seki, J., & Hasegawa, H. (1983). The heterogeneous condensation of interstellar ice grains.
994 *Astrophysics and Space Science*, *94*(1), 177-189. https://doi.org/10.1007/BF00651770

995 Smith, I. W. M. (1980). *Kinetics and Dynamics of Elementary Gas Reactions*. Butterworths.

996 Span, R., & Wagner, W. (1996). A New Equation of State for Carbon Dioxide Covering the Fluid
997 Region from the Triple-Point Temperature to 1100 K at Pressures up to 800 MPa. *Journal*
998 *of Physical and Chemical Reference Data*, *25*(6), 1509-1596.
999 https://doi.org/10.1063/1.555991

1000 Stcherbinine, A., Vincendon, M., Montmessin, F., Wolff, M. J., Korablev, O., Fedorova, A.,
1001 Trokhimovskiy, A., Patrakeev, A., Lacombe, G., Baggio, L., & Shakun, A. (2020). Martian
1002 Water Ice Clouds During the 2018 Global Dust Storm as Observed by the ACS-MIR
1003 Channel Onboard the Trace Gas Orbiter [https://doi.org/10.1029/2019JE006300]. *Journal*
1004 *of Geophysical Research: Planets*, *125*(3), e2019JE006300.
1005 https://doi.org/https://doi.org/10.1029/2019JE006300

1006 Takagi, S., Mahieux, A., Wilquet, V., Robert, S., Vandaele, A. C., & Iwagami, N. (2019). An
1007 uppermost haze layer above 100 km found over Venus by the SOIR instrument onboard
1008 Venus Express. *Earth, Planets and Space*, *71*(1), 124. https://doi.org/10.1186/s40623-019-
1009 1103-x

1010 Titov, D. V., Ignatiev, N. I., McGouldrick, K., Wilquet, V., & Wilson, C. F. (2018). Clouds and
1011 Hazes of Venus. *Space Science Reviews*, *214*(8), 126. https://doi.org/10.1007/s11214-018-
1012 0552-z

1013 Turco, R. P., Toon, O. B., Whitten, R. C., & Keesee, R. G. (1983). Venus: Mesospheric hazes of
1014 ice, dust, and acid aerosols. *Icarus*, *53*(1), 18-25. https://doi.org/10.1016/0019-
1015 1035(83)90017-9

1016 Warren, S. G. (1986). Optical constants of carbon dioxide ice. *Applied Optics*, *25*(16), 2650-2674.
1017 https://doi.org/10.1364/AO.25.002650

1018 Warren, S. G., & Brandt, R. E. (2008). Optical constants of ice from the ultraviolet to the
1019 microwave: A revised compilation. *113*(D14). https://doi.org/10.1029/2007JD009744

1020 Wilquet, V., Drummond, R., Mahieux, A., Robert, S., Vandaele, A. C., & Bertaux, J.-L. (2012).
1021 Optical extinction due to aerosols in the upper haze of Venus: Four years of SOIR/VEX
1022 observations from 2006 to 2010. *Icarus*, *217*(2), 875-881.
1023 https://doi.org/https://doi.org/10.1016/j.icarus.2011.11.002

1024 Wilquet, V., Fedorova, A., Montmessin, F., Drummond, R., Mahieux, A., Vandaele, A. C., Villard,
1025 E., Korablev, O., & Bertaux, J. L. (2009). Preliminary characterization of the upper haze
1026 by SPICAV/SOIR solar occultation in UV to mid-IR onboard Venus Express
1027 [https://doi.org/10.1029/2008JE003186]. *Journal of Geophysical Research: Planets*,
1028 *114*(E9). https://doi.org/https://doi.org/10.1029/2008JE003186

1029 Wölk, J., Wyslouzil, B. E., & Strey, R. (2013). Homogeneous nucleation of water: From vapor to
1030 supercooled droplets to ice. *AIP Conference Proceedings*, *1527*(1), 55-62.
1031 https://doi.org/10.1063/1.4803203

1032 Wood, S. E. (1999). *Nucleation and growth of carbon dioxide ice crystals in the Martian*
1033 *atmosphere* [Ph.D., University of California, Los Angeles]. ProQuest Dissertations &
1034 Theses A&I. http://0-
1035 search.proquest.com.wam.leeds.ac.uk/docview/304496329?accountid=14664
1036 http://openurl.ac.uk/?genre=dissertations+%26+theses&issn=&title=Nucleation+and+gro
1037 wth+of+carbon+dioxide+ice+crystals+in+the+Martian+atmosphere&volume=&issue=&
1038 date=1999-01-
1039 01&atitle=&spage=&aulast=Wood&sid=ProQ:ProQuest+Dissertations+%26+Theses+A
1040 %26I&isbn=9780599260795&jtitle=&btitle=&id=doi:

1041